

THE STRUCTURE, ENERGETICS AND MELTING BEHAVIOR OF
FREE PLATINUM CLUSTERS

A THESIS SUBMITTED TO
THE GRADUATE SCHOOL OF NATURAL AND APPLIED SCIENCES
OF
THE MIDDLE EAST TECHNICAL UNIVERSITY

BY

ALİ SEBETCİ

IN PARTIAL FULFILLMENT OF THE REQUIREMENTS FOR THE DEGREE OF

DOCTOR OF PHILOSOPHY

IN

THE DEPARTMENT OF PHYSICS

JANUARY 2004

Approval of the Graduate School of Natural and Applied Sciences.

Prof. Dr. Canan Özgen
Director

I certify that this thesis satisfies all the requirements as a thesis for the degree of Doctor of Philosophy.

Prof. Dr. Sinan Bilikmen
Head of Department

This is to certify that we have read this thesis and that in our opinion it is fully adequate, in scope and quality, as a thesis for the degree of Doctor of Philosophy.

Prof. Dr. Ziya B. Güvenç
Co-Supervisor

Assoc. Prof. Dr. Hatice Kökten
Supervisor

Examining Committee Members

Prof. Dr. Ziya B. Güvenç

Prof. Dr. Süleyman Özçelik

Prof. Dr. Şinasi Ellialtıoğlu

Assoc. Prof. Dr. Hatice Kökten

Dr. Sadi Turgut

ABSTRACT

THE STRUCTURE, ENERGETICS AND MELTING BEHAVIOR OF FREE PLATINUM CLUSTERS

Sebetci, Ali

Ph. D., Department of Physics

Supervisor: Assoc. Prof. Dr. Hatice Kökten

Co-Supervisor: Prof. Dr. Ziya B. Güvenç

JANUARY 2004, 96 pages

The Voter and Chen version of an embedded-atom model, derived by fitting to experimental data of both the diatomic molecule and bulk platinum simultaneously, has been applied to study the locally stable structures, energetics, growth patterns and the melting behavior of free platinum clusters in the size range of $N=2-56$ and $N=75$. Using the constant-energy molecular dynamics simulation, thermal and conjugate-gradient minimization techniques, the global minima and the other locally stable structures have been distinguished from those stationary structures that correspond to saddle points of

the potential energy surface. The number of isomers and the probabilities of sampling different basins of attractions of the clusters from 2 to 22 atoms are obtained. The energy spectra of these clusters have been analyzed. The correlations between the total energy of the 75-atom cluster and the isomer number and the energy-spectrum-width of the isomers are investigated. The number of isomers of 75-atom cluster as a function of total energy is presented, and the isomer probability distribution is discussed. The melting behavior of Pt_N clusters in the size range of $N=12-14$, 54-56 and $N=75$ has been studied. An atom-resolved analysis method including physical quantities such as the root-mean-square bond-length fluctuation and coordination number for individual atoms as functions of temperature has been presented. Comparisons have been made with the results of previous calculations using electronic structure and empirical potential methods. The results show that the global minima have structures based on either octahedral, decahedral or icosahedral packing. Some of the icosahedral global minima do not have a central atom. The 54-atom icosahedron without a central atom is found to be more stable than the 55-atom complete icosahedron. The lowest energy structures are not always the most probable isomers for each size. The global minimum structures of Pt clusters do not melt at a specific temperature, rather, melting processes take place over a finite temperature range. While some of the clusters exhibit one-stage melting, some of them undergo two-stage melting as the temperature increases. The specific heat of the clusters in the liquid phase is higher than that of the solid form.

Keywords: metal clusters, embedded-atom method, molecular dynamics, melting, phase change

ÖZ

PLATİN ATOM TOPAKLARININ YAPISI, ENERJİSİ VE ERİME BİÇİMLERİ

Sebetci, Ali

Doktora, Fizik Bölümü

Tez Yöneticisi: Assoc. Prof. Dr. Hatice Kökten

Ortak Tez Yöneticisi: Prof. Dr. Ziya B. Güvenç

Ocak 2004, 96 sayfa

Aynı anda hem iki atomlu platin molekülünün hem de kristal yapıdaki platinin deneysel verilerine uyacak şekilde üretilen gömülü atom metodunun Voter-Chen versiyonu, 2 ile 56 arasında ve 75 atoma sahip serbest platin topaklarının yapılarının, enerjilerinin, büyüme yollarının ve erime biçimlerinin çalışılması için kullanıldı. Sabit enerjili moleküler dinamik simülasyonu, sıcaklık düşürme ve eşlenik-gradyant minimizasyon teknikleri kullanılarak en düşük enerji yapıları ve diğer bölgesel kararlı yapılar, potansiyel enerji yüzeyinin eyer noktalarına (saddle points) karşılık gelen yapılardan ayrıldı. 2 ile 22 arasında

atoma sahip topakların izomer sayısı ve her bir izomerin temsil edilme olasılığı hesaplandı. Bu topakların enerji spektrumları analiz edildi. 75 atomlu topağın toplam enerjisi ile izomer sayısı ve enerji spektrum aralılığı arasındaki ilişki araştırıldı. Bu topağın izomer sayısı toplam enerjisinin bir fonksiyonu olarak sunuldu ve izomerlerin temsil edilme olasılıkları çalışıldı. 12-14, 54-56 ve 75 atomlu topakların erime şekilleri araştırıldı. Sıcaklık değişimiyle her bir atomun bağ uzunluğundaki değişimin *rms* değeri ve her bir atomun komşu sayısındaki değişim gibi fiziksel nitelikleri içeren bir analiz metodu sunuldu. Elektriksel yapı ve deneysel potansiyel metodları ile elde edilmiş daha önceki sonuçlarla karşılaştırmalar yapıldı. Elde edilen sonuçlar gösterdi ki en düşük enerji yapıları octahedral, decahedral veya icosahedral yapı biçimlerinden birine sahiptir. Bazı icosahedral en düşük enerji yapıları merkezlerinde hiç bir atom içermemektedir. 54 atomlu merkezi boş icosahedron, 55-atomlu merkezi dolu icosahedrondan daha karardır. En düşük enerji yapıları her zaman temsil edilme olasılığı en yüksek yapılar olmak zorunda değildir. Platin atom topakları kesin bir sıcaklıkta erimezler, aksine erime süreci belli bir sıcaklık aralığında gerçekleşir. Bazı topaklar tek aşamalı erime gösterirken diğer bazıları iki aşamalı erime gösterir. Bir topağın sıvı haldeki öz ısı katı haldekinden daha büyüktür.

Anahtar Kelimeler: metal atom topakları, gömülü atom metodu, moleküler dinamik, erime, faz değişimi

To My Wife

ACKNOWLEDGMENTS

I would firstly like to thank my supervisor Prof. Ziya B. Güvenç for his indispensable support and guidance throughout the whole study. I would also like to thank my co-supervisor Assoc. Prof. Hatice Kökten for her help. I would finally like to thank to my wife not only for her patience and understanding but also for her support and encouragement.

PREFACE

There are considerable theoretical and experimental interest in the study of gas phase and surface-deposited metal clusters in the last few decades, for a number of reasons. The use of clusters as components of nanodevices is one of the most important reasons. Due to their finite size, these small particles may have totally different structures and material properties than their bulk crystalline counterparts. Furthermore, these properties may sometimes change drastically whenever a single atom is added to or removed from the cluster. This opens the pathway for a whole new world of tailor made materials in the future.

In this study, I try to help a fundamental understanding of three of the most important properties of platinum clusters, namely, their structure, dynamics, and thermodynamics.

TABLE OF CONTENTS

ABSTRACT	iii
ÖZ	vi
DEDICATION	viii
ACKNOWLEDGMENTS	ix
PREFACE	x
TABLE OF CONTENTS	xi
LIST OF TABLES	xiii
LIST OF FIGURES	xiv
LIST OF SYMBOLS	xvi
CHAPTER	
I INTRODUCTION	1
I.1 Cluster Science	1
I.2 Aim and Scope of The Thesis	3
II METHODOLOGY	5
II.1 Voter-Chen Potential	7
II.2 Computational Procedure	8
III $Pt_2 - Pt_{21}$ CLUSTERS	11
III.1 Literature	11
III.2 Structures	13
III.3 Isomers and Simple Growth Paths	22
III.4 Probabilities	30

IV	$Pt_{22} - Pt_{56}$ CLUSTERS	39
IV.1	Computational Details	39
IV.2	Global Minima	44
V	MELTING BEHAVIOR OF THE CLUSTERS	57
V.1	Computational Details	57
V.2	Results	58
VI	Pt_{75} CLUSTER	71
VI.1	Computational Details	71
VI.2	Isomers and Isomer Spectrum	73
VI.3	Phase Changes and Melting	78
VII	CONCLUSIONS	85
	REFERENCES	88
	VITA	94

LIST OF TABLES

II.1	Properties of the bulk platinum and the diatomic platinum molecule	8
III.1	Results of 10,000 independent initial configurations for $Pt_2 - Pt_{21}$	14
III.2	Total energies (eV) for all isomers of $Pt_6 - Pt_8$ and for the first 8 isomers of $Pt_9 - Pt_{21}$	29
III.3	Probabilities of all isomers of $Pt_6 - Pt_8$ and the first 9 isomers of $Pt_9 - Pt_{21}$	31
III.4	The probabilities of sampling the isomers of Pt_9 clusters obtained by quenching 1900 K, 2600 K, 3000 K, 3500 K, and 4000 K initial configurations	31
IV.1	Results for global minima of $Pt_{22} - Pt_{56}$ clusters	45
IV.2	Coordination number analysis of $Pt_{22} - Pt_{56}$ clusters	51
VI.1	Energies of the first 14 isomers of the Pt_{75} cluster at T=0 K . .	74

LIST OF FIGURES

III.1	Lowest energy structures of $Pt_2 - Pt_{21}$ clusters	15
III.2	(a):Binding energy per atom ($E_l/atom$) for the global minima of $Pt_2 - Pt_{21}$ clusters (b):First (D_1) and second differences (D_2) in the lowest energies of $Pt_2 - Pt_{21}$ clusters	21
III.3	(a):The number of isomers N_i versus cluster size N graph (b):The width of the energy spectrum $ESW/atom$ versus cluster size N graph	23
III.4	All locally stable structures of $Pt_6 - Pt_9$ clusters other than the global minima	25
III.5	The $2^{nd} - 6^{th}$ locally stable structures of the $Pt_{10} - Pt_{15}$ clusters	26
III.6	Some locally stable structures of $Pt_{16} - Pt_{21}$ clusters	27
III.7	Growth pattern of the locally stable structures of small Pt clusters. * denotes the most probable isomers	28
III.8	The probability distributions of the isomers of $Pt_6 - Pt_{13}$ clusters obtained by quenching 2600 K initial configurations	33
III.9	The probability distributions of the isomers of $Pt_{14} - Pt_{21}$ clusters obtained by quenching 2600 K initial configurations	34
IV.1	The short-time average internal kinetic energies versus time graphs of Pt_{55} clusters (a) for the first candidate at 297 K, (b) for the second candidate at 969 K, (c) for the global minimum structure at 979 K	40
IV.2	(a) Energies where $E_0 = 13.1113 - 11.2291N^{1/3} + 6.73356N^{2/3} - 6.20365N$ (b) The second finite difference in binding energy . . .	47
IV.3	Global minima for $Pt_{22} - Pt_{39}$ clusters	48
IV.4	Global minima for $Pt_{40} - Pt_{56}$ clusters	49
V.1	Heating process of Pt_{12} cluster	60
V.2	Heating process of Pt_{13} cluster	62
V.3	Heating process of Pt_{14} cluster	63
V.4	Heating process of Pt_{54} cluster	65
V.5	Heating process of Pt_{55} cluster	67
V.6	Heating process of Pt_{56} cluster	69
VI.1	The 1^{st} , 2^{nd} , 3^{rd} , and 7^{th} locally stable structures of the Pt_{75} cluster	72

VI.2	Correlations between isomer-energy-spectrum and isomer number with temperature	75
VI.3	Isomer number versus isomer energy in units of eV	77
VI.4	Short-time averaged temperatures as a function of time interval	79
VI.5	Time averaged atomic RMS bond-length fluctuations as a function of temperature	80
VI.6	Time averaged potential energies of all of the atoms as a function of temperature	81
VI.7	Time averaged coordination numbers as a function of temperature	82
VI.8	Caloric curve of the Pt_{75}	83
VI.9	Specific heat versus temperature of the Pt_{75}	84

LIST OF SYMBOLS

ADF	Amsterdam density functional	LDA	local density approximations
CASSCF	complete active space self consistent-field	MC	Monte Carlo
CG	conjugate gradient	MC-CEM	Monte Carlo-corrected ef- fective medium theory
CN	coordination number	MD	molecular dynamics
DF	density functional	PES	potential energy surface
EAM	embedded-atom method	RMS	root mean square
ESW	energy spectrum width	STKE	short-time average internal kinetic energies
FOCI	first-order configuration in- teraction	TQ	thermal quenching

CHAPTER I

INTRODUCTION

I.1 Cluster Science

In general, interest on the area of atomic clusters has grown rapidly within the last three decades not only because of their unique, size dependent structures and properties different from those of the bulk, but also their central position between molecules on the one hand and condensed matter on the other. A systematic study of evolution of these properties with size allows elucidation of the transition from the molecular structure to condensed matter phase. Clusters, in particular metal clusters, play an important role in many chemical reactions as catalysts. The structure of small metal clusters in a reaction can have a major effect on the rate of formation of products [1]. Because of, at least, above reasons there are considerable numbers of experimental and theoretical studies on clusters in the literature [2, 3, 4, 5, 6, 7, 8, 9].

A cluster is an aggregation of a countable number of particles which can

contain from a few to tens of thousands of atoms or molecules. The bonding forces in a cluster can be metallic, covalent, ionic, hydrogen-bonded or Van der Waals in character. These clusters may be studied in the gas phase, in a molecular beam, absorbed onto a surface or trapped in an inert matrix.

It is possible to form, for instance, the transition metal clusters in the gas phase, where they can be cooled to low internal energies. After such species have been formed and cooled, their electronic and molecular architecture can be probed in detail using various elegant spectroscopies, such as resonant two-photon ionization (R2PI) [10, 11, 12] and dissociation spectroscopies (R2PD) [13], laser-induced fluorescence (LIF) [14, 15, 16, 17], and photoelectron spectroscopy (PES) [18, 19, 20]. The structure of the clusters deposited on a surface can be probed by techniques such as high resolution electron microscopy [21], and scanning tunneling microscopy [22, 23]. However, the effects of the surface on the cluster have then to be taken into account.

It can be said that the field of nanoscience and nanotechnology - the study and fabrication of structures and devices on the nanometer scale (10^{-9} m) - has been derived from a famous talk by Richard Feynman in 1959 [24]. In his talk, entitled *There's Plenty of Room at the Bottom*, he challenged scientists to develop a new field of study where devices and machines could be constructed from components consisting of a small number (tens or hundreds) of atoms. This article has inspired generations of physicists and chemists to try to make Feynman's vision a reality and there are now a large number of nanoscience laboratories in universities and institutes throughout the world [6]. The new

hopes and the dreams of the nanotechnology are the most recent reasons for the increased interest in clusters. The present state of the knowledge of the properties of the clusters of atoms which in their bulk form conventional metals or semiconductors can be found in Ref. [25].

I.2 Aim and Scope of The Thesis

The aim of this thesis is to help a fundamental understanding of three of the most important properties of clusters: structure, dynamics, and thermodynamics. In this theoretical study, we have chosen the transition metal platinum as our specific example and describe it by the Voter-Chen version [26] of the embedded-atom method (EAM) potential. We did our calculations for the Pt_N clusters in the size range of $N=2-56$ and $N=75$.

Platinum, rhodium, and palladium have been used very extensively in heterogeneous catalysis, especially for the reactions involving CO and H_2 . They are used, for instance, in automotive exhaust systems to reduce toxic pollutants such as CO , NO , and hydrocarbons. Platinum clusters have small hydrogenation energy compared to other metal clusters [27].

After presenting the details of the interaction potential and the computational procedure in Chapter II, the global minimum energy structures, the growth pathways, the number of isomers, the probabilities of sampling different basins of attractions, and the energy spectra of the isomers of $Pt_2 - Pt_{21}$ clusters are presented in Chapter III. The global minima of the clusters $Pt_{22} - Pt_{56}$ are discussed in Chapter IV. The melting behavior of the icosahedral clusters

with 12-14 and 54-56 atoms is discussed in Chapter V. The global minimum energy structure and a detailed study of the isomers and their energetics as well as the melting behavior of the Pt_{75} cluster is presented in Chapter VI. Finally, in the conclusion we summarize the results obtained in this work, and suggest some possible future directions.

CHAPTER II

METHODOLOGY

The theoretical studies of atomic clusters can be classified into two groups as density functional *ab initio* methods, and the model and the empirical potentials for the simulations. *Ab initio* techniques seek to calculate the properties of a system from first principles with no parameterizations. The advantage of the first group methods is that in principle they can provide highly accurate results. However, these approaches are much more computationally expensive than empirical potentials. The pair interaction potentials such as the Lennard-Jones [28] or the Morse [29] potentials on the other hand, are not adequate to characterize the metals. Pair potentials fail to predict the Cauchy violation for cubic solids where the elastic constants C_{12} and C_{44} are different (for a pair potential C_{12} is always equal to C_{44}). Pair potentials fail to predict the inward relaxation of the outer layer of atoms at a metal surface. The ratio of the vacancy energy, E_{vac} , which is the energy needed to remove an atom from the bulk and place it on the surface, to the cohesive energy, E_{coh} , which is the

energy of an atom in the bulk, is always overestimated by a pair potential as it does not account for the effect of the local coordination environment at the vacancy on the bonding (for a pair potential $E_{vac} \equiv E_{coh}$). Pair potentials also tend to favor more highly connected systems, preferring fcc and hcp coordination over bcc systems and disfavoring low coordination environments such as the diamond structure [8].

There are two main approaches for including many-body character in the bonding scheme. One can employ an explicit description of higher order terms such as 3-body or 4-body terms in the potential energy series or one can introduce many-body character through a dependency on the local electronic density. The Axilrod-Teller potential [30] and the Murrell-Mottram potential [31] can be given as the examples of the first approach. Density dependent potentials introduce a term which describes the binding in terms of the local electron densities at each atom. The local electron density is dependent on the configuration of the whole system and this introduces a many-body component into the bonding. The Finnes-Sinclair potential [32], The Sutton-Chen potential [33], the Gupta potential [34] and the EAM potential [35] are the most popular ones of this type.

In this study the *Pt* clusters are characterized by a semi-empirical Voter and Chen [26] version of the EAM. The virtue of Voter and Chen version is that it is derived by fitting the EAM to both the basic bulk properties of the *Pt* and to the bond length and bond energy of the diatomic molecule *Pt*₂ simultaneously [36, 37, 38]. This potential energy surface gives perfect

agreement with the experimental values of the equilibrium lattice constant, the bulk modulus and the crystal cohesive energy (E_{coh}) and it also produces reasonably well values of the properties such as unrelaxed vacancy formation energy (E_{vac}^f) and the three cubic elastic constants (C_{11} , C_{12} and C_{44}) for the following seven fcc metals: Ni, Pd, Pt, Cu, Ag, Au and Al [26]. Therefore this EAM may have a wide range of validity from a few atoms to the larger sizes of the Pt_N clusters.

II.1 Voter-Chen Potential

In any N -scaling energy expression, the total energy, E_{tot} of a system of N atoms can be written as a sum

$$E_{tot} = \sum_i^N E_i. \quad (\text{II.1})$$

In the EAM, the configuration energy E_i of each atom i is represented as

$$E_i = \frac{1}{2} \sum_{j \neq i} \phi_{ij}(r_{ij}) + F_i(\bar{\rho}_i), \quad (\text{II.2})$$

where F_i is the embedding term, ϕ_{ij} is the pairwise-addition part of the interaction between atoms i and j , r_{ij} is the distance between atoms i and j , and $\bar{\rho}_i$ is the total "host" electron density at the position of atom i :

$$\bar{\rho}_i = \sum_{j \neq i} \rho_j(r_{ij}). \quad (\text{II.3})$$

The sums over neighboring atoms j are limited by the range of the cutoff for ϕ and ρ , which is generally one to four neighbor shells in the perfect crystal. $F(\bar{\rho})$ provides a many-body contribution to the energy. The key to EAM is the

Table II.1: Properties of the bulk platinum and the diatomic platinum molecule

	C_{11}^a	C_{12}^a	C_{44}^a	$E_{vac}^f(eV)$	$D_e(eV)$	$R_e(\text{\AA})$
experimental	3.47	2.51	0.77	1.5	3.17	2.45
calculated	3.21	2.64	0.78	1.49	3.15	2.34

^a $10^{12} \text{ erg cm}^{-3}$

nonlinearity of the function $F(\bar{\rho})$. If F were purely linear, the two terms in Eq. (II.2) could be collapsed to give a simple pair potential. Thus, a nonlinear $F(\bar{\rho})$ provides a many-body contribution to the energy. Because $\bar{\rho}_i$ depends only on scalar distances to neighboring atoms, the many-body term has no angular dependence. Nonetheless, this spherically symmetric, many-body interaction is quite important.

All the parameters in the Voter and Chen model were determined by minimizing the root-mean-square deviation (χ_{rms}) between the calculated and experimental values of three elastic constants (C_{11} , C_{12} , and C_{44}), and the unrelaxed vacancy formation energy (E_{vac}^f) of the bulk platinum and of the bond length (R_e) and bond strength (D_e) of the diatomic molecule. The experimental data used in the fitting process along with the calculated values can be found in Table II.1.

II.2 Computational Procedure

Once one has a description of the interaction in a system, one can look for stable configurations within that system. Many techniques have been developed for searching the potential energy surface to find the lowest energy configuration or global minimum: Simulated annealing techniques model the slow quenching

of a cluster from a high temperature configuration into low energy conformation while probing the thermally accessible regions of phase space [39]. The evolution of the system can be performed using either Monte Carlo (MC) or molecular dynamics (MD) techniques. The MC basin hopping algorithm has been developed by Doye and Wales [40]. This algorithm combines local minimizations with MC sampling techniques. The local minimizations transform the potential energy surface into a series of basins of attraction. Searching the transformed potential energy is simpler than searching the original surface. Genetic algorithms have been developed to study cluster structure [41, 42, 43, 44]. These algorithms borrow ideas from natural evolution to search for the global minimum on the potential energy surface.

The random search algorithm, which we have employed for Pt_N ($N=2-21$) clusters in this study, is a simple method to determine the global minimum on a potential energy surface. A large number of random configurations of atoms are subjected to the thermal quenching (TQ) simulations to obtain the equilibrium structural forms of the clusters. The random initial configurations are produced by recording the atomic coordinates along a constant-energy MD trajectory.

In our calculations, 10,000 independent initial configurations are generated by recording phase-space coordinates at every 500 MD simulation steps along high-energy trajectories. The chosen internal energies (about 2600 K) are much higher than the typical melting temperatures of the clusters (the melting temperature of the bulk platinum is 2041 K) so that initial configurations can

sample as many points as possible in the $6N$ dimensional phase-space. The TQ of these configurations were completed by setting the internal kinetic energies of the clusters to zero at every 50 or 100 simulation steps until the internal kinetic energies are completely removed. Thus, the locally stable isomers are separated from those metastable ones, saddle points of the potential energy surface (PES). Hamilton's equation of motion were solved for all the atoms in a cluster using Hamming's modified 4th order predictor-corrector propagator with a step-size of 10^{-15} s, which guarantees conservation of the total energy of the clusters to within 0.03% – 0.15%.

However, the method of the consideration of a large number of initial configurations is reasonable only for small sizes since the number of isomers of a cluster increases exponentially as the number of atoms in the cluster increases. Thus, the search of the global minima of the larger sizes ($N \geq 22$) has been achieved by including some extra considerations. The details of this search are discussed in Chapter IV. The computational details of the investigation of the melting behavior of the selected size icosahedral clusters and those of the calculations of the Pt_{75} cluster are given in Chapter V and Chapter VI respectively.

CHAPTER III

$Pt_2 - Pt_{21}$ CLUSTERS

III.1 Literature

Experimental studies on small Pt clusters are scarce. The only case of small Pt clusters that has been studied experimentally to our knowledge, is the Pt_2 cluster. Taylor and co-workers [45] used resonant two-photon ionization spectroscopy of jet-cooled Pt_2 to find numerous vibronic bands of it. Jansson and Scullman [46] measured the vibrational spectrum of a Pt_2 in an Ar matrix. Gupta and co-workers [47] were successful in detecting Pt_2 over the temperature range 2259-2739 K.

On the theoretical side, Sachdev et al. [48] studied some of the Pt clusters of 5 to 60 atoms using the EAM of Daw and Baskes [35]. They made a stability analysis where they started with a fixed shape (e.g., an icosahedron) and did a conjugate gradient (CG) minimization [49] to calculate a relaxed shape. Garcia-Rodeja et al. [50] used the Voter and Chen version of the EAM

by carrying out MD simulations to study the structures and melting of 6 fcc transition metals (*Ni*, *Pd*, *Pt*, *Cu*, *Ag*, and *Au*) in the size range of $N=2-23$. However, they did not present neither the stable isomeric forms, nor their probabilities of sampling. Yang and DePristo [51] performed the MD/Monte Carlo, corrected effective medium theory (MD/MC-CEM) [52] to study only 13-atom *Pt* clusters using two different interatomic potentials. Doye and Wales [53] reported the global minima for metal clusters modelled by the Sutton-Chen [33] family of potentials containing up to 80 atoms, using a Monte Carlo minimization global optimization algorithm [54]. They did not present the other low energy minima, and their probabilities of sampling, either. Finally, Johnston and co-workers [55] have reported the global minima for *Pt*, *Pd* and *Pt* – *Pd* bimetallic clusters using the many-body Gupta potential in their genetic algorithm calculations.

There are also a few *ab initio* studies on the small *Pt* clusters. Ellis et al. [56] studied the *Pt*₄ cluster using an *ab initio* generalized valence bond method within the relativistic effective core potential and a double-zeta basis. Complete active space self consistent-field (CASSCF) calculations followed by the first-order configuration interaction (FOCI) computations has been performed by Balasubramanian [27] on the *Pt*₂ and by Dai and Balasubramanian [57] on the *Pt*₄ clusters to study their electronic structures. Yang and co-workers [58] applied the non-self consistent Harris functional version [59] of the local density approximations (LDA) within density functional (DF) theory to obtain minimum energy structures of the *Pt*_{*N*} clusters for $N=2-6$. For-

tunelli [60] has performed DF calculations on the small Pt_N clusters ($N=1-4$) by using Amsterdam Density Functional (ADF) set of programs [61]. Finally, Apra and Fortunelli [62] have performed DF calculations on Pt_{13} and Pt_{55} cuboctahedral clusters by using DF theory module of the NW-Chen computational chemistry package [63].

III.2 Structures

The number of isomers (N_i), the lowest binding energies per atom (E_l/atom), the average bond lengths (R_b), and the energy spectrum widths (ESW) of $Pt_2 - Pt_{21}$ clusters are given in Table III.1. The minimum energy geometries of these clusters are presented in Fig. III.1. Except the first three structures, each of these clusters has one or more of the trigonal, tetragonal, pentagonal or hexagonal bipyramid forms as a main sustaining part. Therefore, it is possible to classify them with respect to their backbones. We call $Pt_2 - Pt_4$ group as primitive. The Pt_5 is the only one belonging to trigonal bipyramid group. The tetragonal bipyramid group consists of the lowest energy structures of the Pt_6 and Pt_8 clusters. In the pentagonal bipyramid group, there are Pt_7 , $Pt_9 - Pt_{14}$ and Pt_{19} clusters. The $Pt_{15} - Pt_{18}$, Pt_{20} and Pt_{21} clusters are in hexagonal bipyramid group. We now discuss the structures and energetics of the Pt clusters in ten steps.

Pt_2 : The bond energy and the bond length of the Pt dimer are 3.15 eV and 2.34 Å, respectively. The value for the bond energy is in excellent agreement with the experimental value 3.14 ± 0.02 eV measured by Taylor et al. [45], since

Table III.1: Results of 10,000 independent initial configurations for $Pt_2 - Pt_{21}$

N^a	N_i^b	$E_l/atom(eV)^c$	$R_b(\text{\AA})^d$	$ESW/atom(eV)^e$
2	1	1.58	2.34	0
3	1	2.45	2.41	0
4	1	3.12	2.46	0
5	1	3.44	2.49	0
6	2	3.74	2.50	0.11
7	4	3.89	2.53	0.15
8	8	3.99	2.52	0.18
9	17	4.08	2.56	0.20
10	29	4.16	2.57	0.22
11	59	4.22	2.58	0.19
12	147	4.30	2.60	0.22
13	76	4.43	2.61	0.20
14	322	4.41	2.62	0.21
15	253	4.46	2.64	0.23
16	364	4.49	2.63	0.22
17	423	4.52	2.65	0.22
18	541	4.54	2.64	0.18
19	849	4.57	2.64	0.20
20	1767	4.59	2.63	0.19
21	1847	4.61	2.66	0.16

^aSize of the cluster

^bNumber of the stable isomers

^cLowest binding energies per atom

^dAverage bond length

^eEnergy spectrum width

the properties of a Pt_2 and those of the bulk Pt were considered simultaneously in the fitting procedure of the PES. Yang et al. [58] have calculated the bond strength and the bond length of the dimer as 3.30 eV and 2.40 Å, respectively, in their *ab initio* studies. Fortunelli [60] has calculated these quantities as 3.70 eV and 2.37 Å, respectively, in his density functional study. Although Yang et al. [58] has reported the dissociation energy of the platinum dimer measured as 3.26 eV, it was the bond strength of the Pt_2^+ ion. Dai and Balasubramanian [57] and Fortunelli [60] have also referred to 3.15 eV as the correct binding total

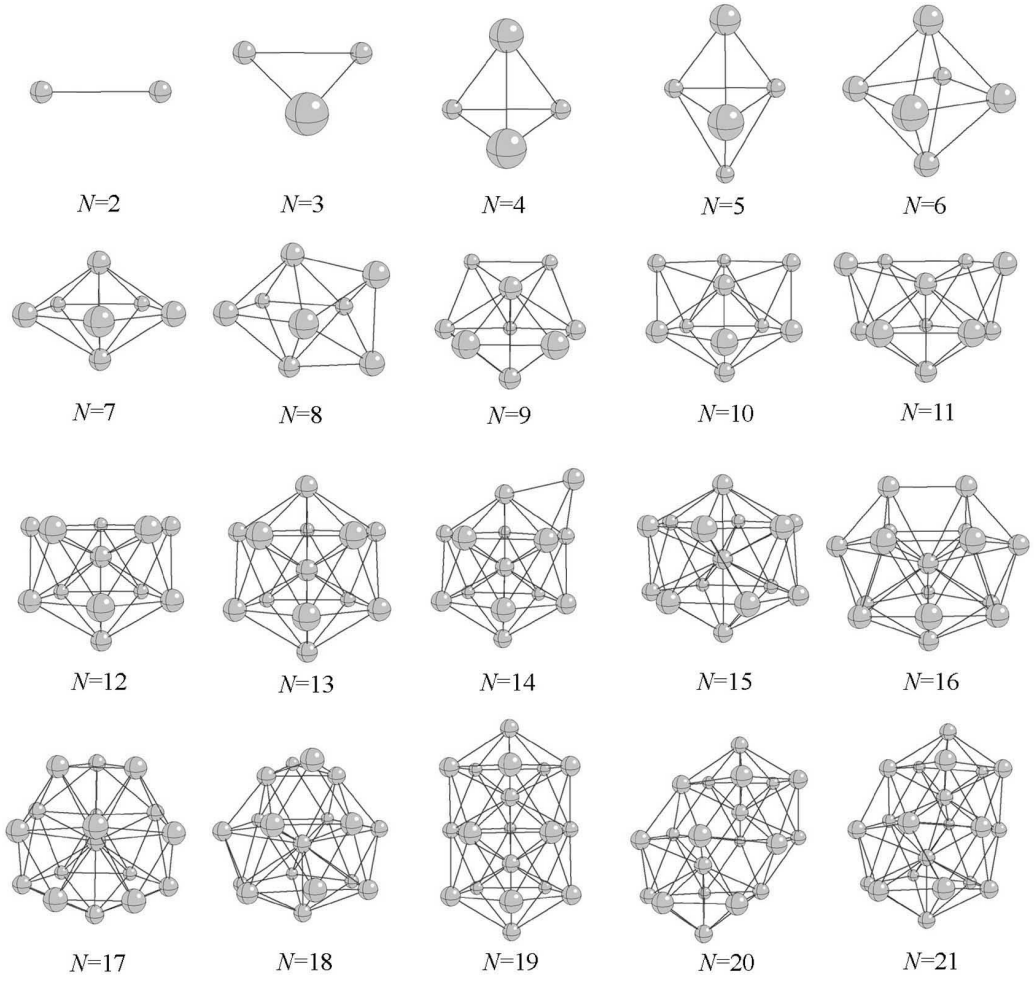


Figure III.1: Lowest energy structures of $Pt_2 - Pt_{21}$ clusters

energy of the Pt dimer. As seen the bond energies and the bond lengths are in good agreement with the experimental value.

Pt_3 : The lowest energy structure of a Pt_3 cluster is an equilateral triangle with a bond length of 2.41 \AA , and energy of 2.45 eV/atom . Yang et al. [58] have also found an equilateral triangle for the least energy structure of the Pt_3 with a bond length of 2.58 \AA , and energy of 2.40 eV/atom . But, they have found two other locally stable structures also: a linear chain, and an isosceles triangle. Fortunelli [60] has found the bond length of the equilateral triangle as

2.54 Å, and the energy as 2.41 eV/atom. He has also mentioned about a linear arrangement. According to our results, the only stable structure of three-atom *Pt* clusters obtained using the TQ technique in 3-D is the equilateral triangle.

Pt₄: Tetrahedral is found to be the lowest energy structure for a *Pt₄*, with a bond length of 2.46 Å, and a binding energy of 3.12 eV/atom. Again we did not find any other stable isomer in 3-D for the *Pt₄*. Dai and Balasubramanian [57] have also reported that a tetrahedral geometry with the 3T_1 electronic state is the ground state of the *Pt₄*. They have given the bond length as 2.60 Å and estimated the binding energy as 2.95 eV/atom, which are in good agreement with our result. They have also found a rhombus and a square as the other locally stable structures similar to the results of Yang et al. [58] and Fortunelli [60]. On the other hand, Yang et al. [58] have reported that the most stable structure for the *Pt₄* is a rhombus of C_{2v} symmetry, with a bond length of 2.64 Å, and a binding energy of 2.56 eV/atom. However, Fortunelli [60] has reported that the most stable structure for the *Pt₄* is a rhombus of D_{2h} geometry, with a bond length of 2.52 Å, and a binding energy of 2.63 eV/atom. In these calculations the tetrahedron structure was unstable, which is not in agreement with the present, and Dai and Balasubramanian [57]’s *ab initio* work.

Pt₅: The largest cluster with a single stable structure in our calculations is the *Pt₅*. A trigonal bipyramid is found to be the least energy structure. The bond length in the equatorial equilateral triangle is 2.52 Å, and all other bond lengths are 2.47 Å. The binding energy of the *Pt₅* cluster is calculated as

3.44 eV/atom. Yang et al. [58] have found a planar structure as the minimum energy structure of the Pt_5 clusters. They have also found a pyramid and a disordered trigonal bipyramid as the other locally stable structures with the binding energies of 2.53 eV/atom and 2.59 eV/atom respectively.

Pt_6 : The Pt_6 is the first size of which we have obtained more than one locally stable structure in our calculations. We will discuss the isomers in the next subsection. The minimum energy geometry of the Pt_6 cluster is a bipyramid with a bond length of 2.50 Å, and a binding energy of 3.74 eV/atom. A bipyramid with a bond length of 2.78 Å, and a binding energy of 2.61 eV/atom was also found by Yang et al. [58] as one of the locally stable structures. They have found 5 distinct stable structures of the Pt_6 . All of these structures are in planar configurations except the bipyramid, and the lowest energy structure consists of four small equilateral triangles, which form a larger equilateral triangle. The lack of some locally stable structures in our results compared to the *ab initio* studies is might be due to that empirical potentials, such as EAM, lack directionality in bonding, which favors dense packets. This effect decreases with increasing number of atoms in the cluster but with the smallest clusters it is influential.

Pt_7 : A pentagonal bipyramid is the most stable structure of Pt_7 clusters. This structure forms the backbone of the icosahedral symmetry. The bond length in the equatorial plane is 2.50 Å, and the bond length between the poles and any atom in the equator is 2.53 Å. The binding energy is calculated as 3.89 eV/atom.

Pt_8 : The lowest energy structure of the Pt_8 can be constructed from the minimum energy structure of the Pt_6 by capping the symmetric two faces of the bipyramid with respect to the equatorial plane, and its energy is 3.99 eV/atom. The average bond lengths are presented in Table III.1.

$Pt_9 - Pt_{14}$: The minimum energy structures of $Pt_9 - Pt_{14}$ clusters have the pentagonal bipyramid as their backbones. It is possible to construct one of them from the previous size by just adding an atom without changing the existing structure. The global minimum energy structures of the first three of these clusters ($Pt_9 - Pt_{11}$) and the icosahedral form of the Pt_{13} are also presented as the global minima by Doye and Wales [53]. However, our results for Pt_{12} and $Pt_{14} - Pt_{21}$ are different from theirs. These differences might be because of the potentials used, which depend on different type of methods employed to describe atomic interactions, and the different computational procedures. Many of the lowest energy geometries of the $Pt_{14} - Pt_{21}$ clusters given by Doye and Wales [53] are found to be some energetically higher locally stable isomers. For instance, the lowest energy structure of the Pt_{14} presented by them is found to be the 4th isomer in our calculations. The lowest energy structure of $N=13$ has a particular importance since it is the first of so called magic numbers (i.e. 13, 55, 147, ...) for icosahedral structures. In an icosahedron with 13 atoms, a central atom is surrounded by 12 atoms, which form a spherical shell. We have calculated the radius of the shell as 2.52 Å. This number has been calculated as 2.50 Å by Sachdev et al. [48]. They have calculated the total binding energy of this geometry as 57.71 eV which is very close to our result

of 57.58 eV. Yang and DePristo [51] have also studied the Pt_{13} clusters with two semi-empirical interatomic potentials. One of the potentials predicted the icosahedral structure with a binding energy of 52.14 eV, the other predicted an open and fluxional structure with a binding energy of 65.66 eV. Sachdev et al. [48] have stated that the magic number icosahedral structures are stable at 0 K, the lowest energy structures of the non-magic number clusters may not be on the icosahedral growth pattern. They have also claimed that magic number structures deform into some disordered structures upon annealing at 300 K. Since, we are going to discuss the dynamical properties and phase transitions of some of the Pt clusters in later chapters, we postpone this discussion to them. Finally, Apra and Fortunelli [62] have studied the Pt_{13} clusters by starting from crystal geometries, i.e. the positions that the atoms assume in the clusters considered as sections of the bulk platinum fcc lattice, and by imposing cuboctahedral symmetry. For the cuboctahedral structure, they found 6.9 eV of binding energy per atom and 2.67 Å of nearest neighbor distance.

$Pt_{15} - Pt_{18}$: In the lowest energy structure of the 15-atom Pt cluster there are two hexagonal bipyramids, which share one of their atoms in the polar region. These two hexagonal planes are rotated with respect to each other like the rotated pentagonal rings in the icosahedral form of the Pt_{13} . Therefore it is not on the icosahedral growth. This hexagonal bipyramid is another building block of higher sizes of the Pt clusters, as we see in the minimum energy structures of $Pt_{16} - Pt_{18}$, Pt_{20} and Pt_{21} . As the size increases from $N=15$ to 18, the atoms accumulate in the same polar region. They form

dimer, trimer, and tetramer, respectively.

$Pt_{19} - Pt_{21}$: When the size of $N=19$ is arrived, the backbone is changed back to the pentagonal bipyramid, and it's structure is a double icosahedron. The central pentagonal bipyramid is shared by the icosahedral forms. The Pt_{20} has an additional atom in its equatorial plane compared to the structure of the Pt_{19} . This additional atom forms a disordered equatorial hexagonal bipyramid as shown in Fig. III.1. In Pt_{21} one of the pentagonal rings near the polar regions is converted into a hexagonal bipyramid ring.

The binding energy per atom of the lowest energy geometries of the $Pt_2 - Pt_{21}$ clusters are plotted as a function of size (N), in Fig. III.2(a). After a rapid initial increase, the lowest energy per atom converges hyperbolically towards the bulk value ($E_{coh}=5.77$ eV) [26] for fcc Pt . An important feature of this graph is the small peak at $N = 13$, corresponding to a region of enhanced stability. Such regions are more evident when the first

$$D_1(N) = E_l(N) - E_l(N - 1), \quad (III.1)$$

and the second

$$D_2(N) = 2E_l(N) - E_l(N - 1) - E_l(N + 1), \quad (III.2)$$

differences in the binding energies are plotted against N as seen in Fig. III.2(b). The second difference in binding energy (D_2) is generally correlated with experimental mass spectral intensities. Fig. III.2(b) indicates that there are pronounced peaks in $D_2(N)$ at $N=4,6$ and 13. The common feature of the least energy structures of these sizes is that they all construct a complete sphere

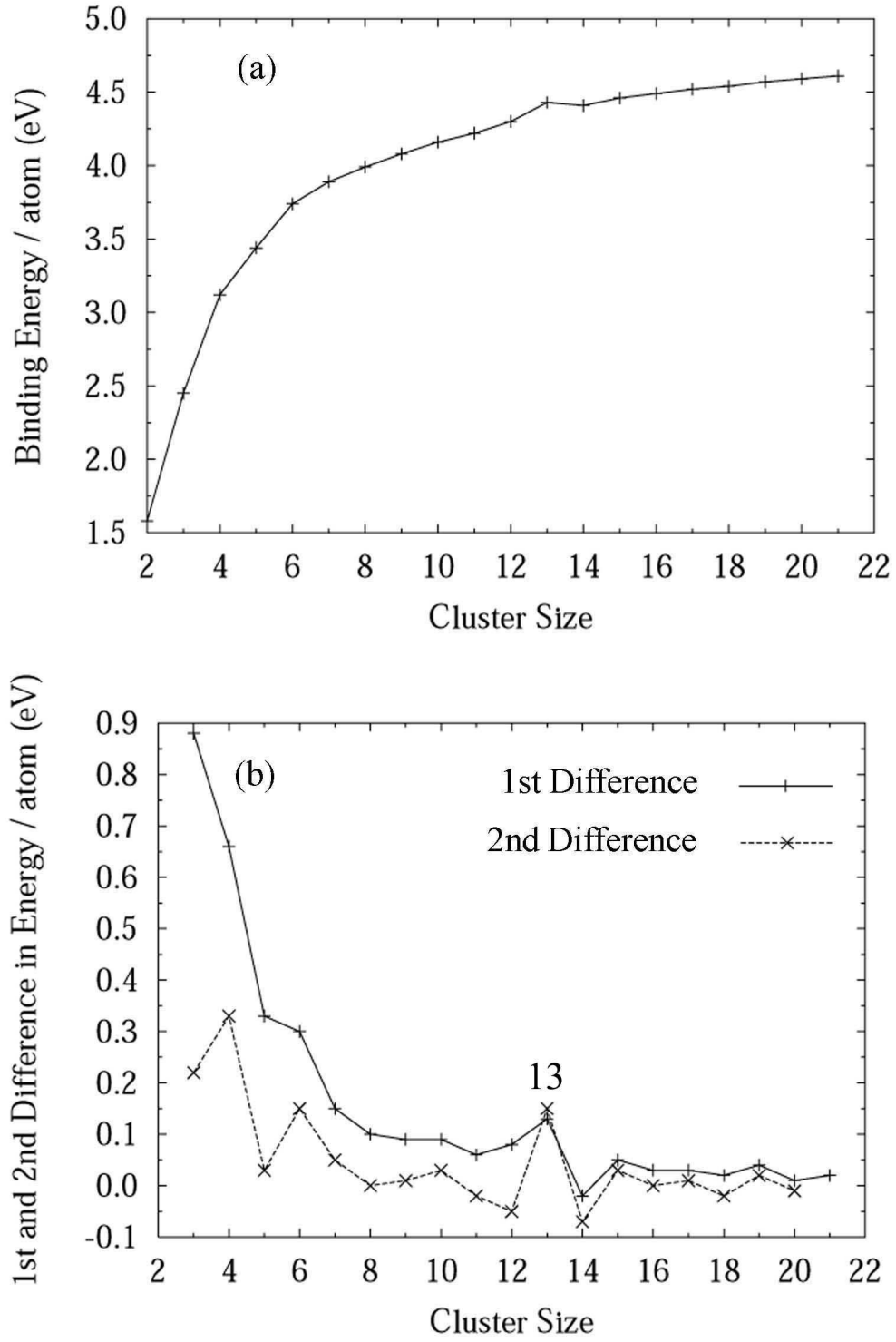


Figure III.2: (a): Binding energy per atom ($E_l/atom$) for the global minima of $Pt_2 - Pt_{21}$ clusters (b): First (D_1) and second differences (D_2) in the lowest energies of $Pt_2 - Pt_{21}$ clusters

where there is no atom at the center for the sizes of $N = 4$ and 6 . However, there exist an atom at the center for the size of $N = 13$. The average bond lengths (R_b) of the lowest energy structures exhibit a similar behavior to the binding energies. They also converge hyperbolically towards the bulk value (2.78 \AA) [64] for fcc Pt .

III.3 Isomers and Simple Growth Paths

The number of stable isomers versus cluster size graph has been plotted in Fig. III.3(a). The number of isomers increases exponentially as the cluster size increases, because of the high dimensionality of the configuration space. The energy spectrum width (ESW/atom) versus cluster size graph has been plotted in Fig. III.3(b). Initially, it increases rapidly, as the cluster size increases ($N \leq 10$). The width of the energy spectrum reaches to the saturation level at $N = 10$. After that the ESW/atom values are oscillating around 0.2 eV . This width is the highest at $N = 15$, 0.23 eV/atom , and the smallest at the size of $N = 21$, 0.16 eV/atom , (for $N \geq 8$). The smaller value for $N = 21$ is might be due to the number of independent initial conditions which is not sufficiently large. For the size range of $N \geq 20$ one should use much larger set of initial conditions for better sampling of the much larger isomer-phase-space.

We have shown all locally stable structures of the $Pt_6 - Pt_9$ clusters other than the global minima in Fig. III.4. We denote the lowest energy structure of a size as $N(1)$ since it is the first isomer, the second isomer is denoted by $N(2)$, and so on. The $2^{nd} - 6^{th}$ locally stable structures of the $Pt_{10} - Pt_{15}$, and $Pt_{16} -$

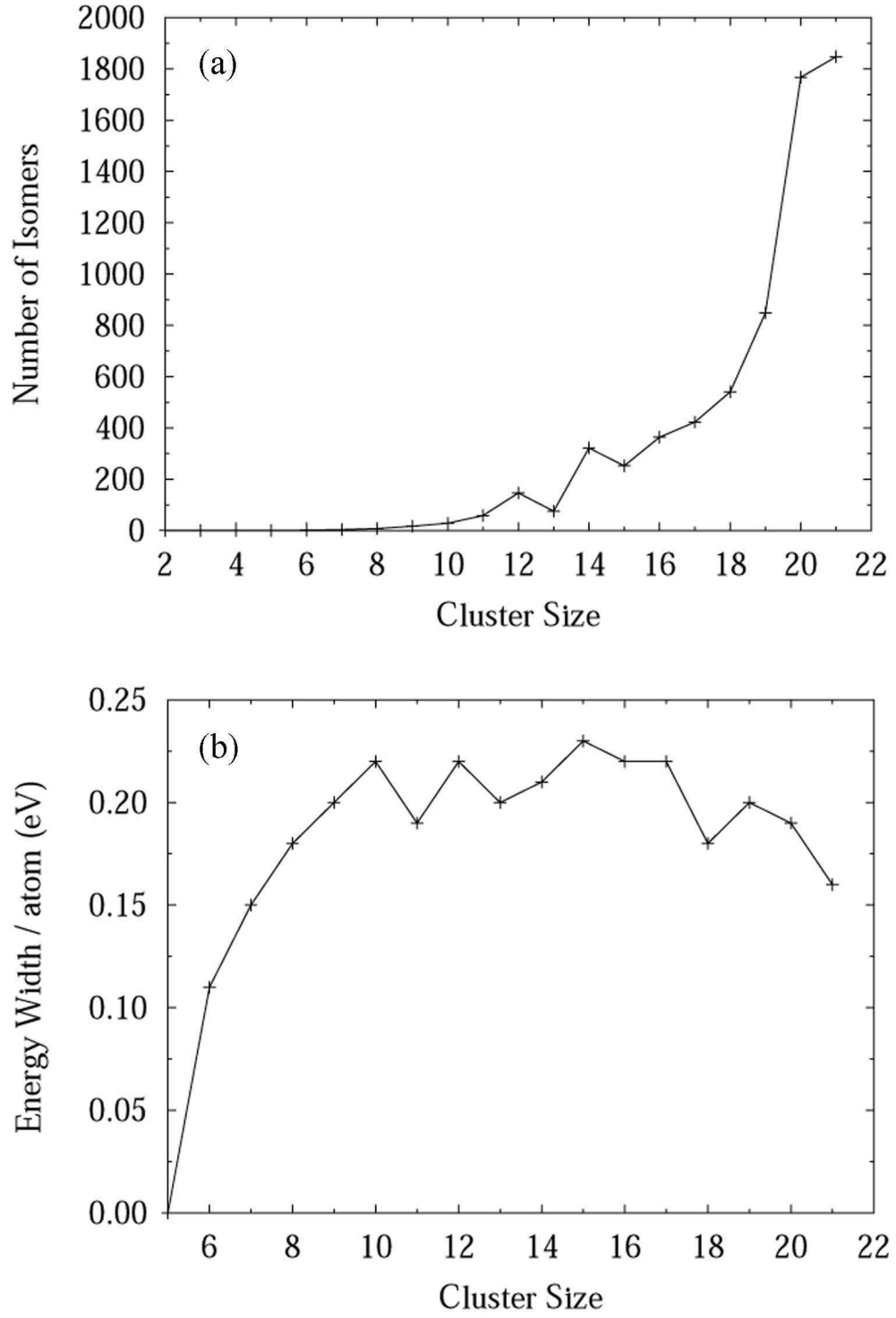


Figure III.3: (a):The number of isomers N_i versus cluster size N graph (b):The width of the energy spectrum ESW/atom versus cluster size N graph

Pt_{21} clusters are given in Figs. III.5 and III.6, respectively. As an exception, we display the 7th and 54th isomers of the Pt_{18} , and Pt_{19} , respectively in Fig. III.6 since they have the highest probability of sampling. It can be seen from the isomer geometries given in Fig. III.1, and Figs. III.4 - III.6 that any structure of a given size can be related to one of the locally stable geometries of the previous size. This relation can occur in two different ways: 1- Either, it is possible to construct the structure of $N(l)$ from a structure of $N-1(l')$ by just adding a new atom to cap one of the faces of existing geometry (e.g., $N=6(2)$ from $N=5(1)$, and $N=7(2)$ from $N=6(1)$). This type of construction nearly preserves the previous interatomic bonds (simple growth path). But, sometimes a few of the bonds can be broken and the previous structure can be disturbed without losing its identity (e.g., $N=10(4)$ from $N=9(3)$ or from $N=9(4)$). 2- Or, instead of going to the top of a face, the new atom is inserted into the ring of the previous structure (e.g., from $N=5(1)$ to $N=6(1)$, and from $N=6(1)$ to $N=7(1)$). Thus, a new building block is constructed.

Sometimes a structure may have a relation to more than one structures of the previous size. For instance, $Pt_9(17)$ can be built from both $Pt_8(7)$ and $Pt_8(8)$. Using the relations described above, we developed a tree diagram in Fig. III.7 showing how the locally stable structures grow. In the diagram the straight lines present the relations of type one, whereas the dotted lines indicate the relations of type two. Since we present the geometries of all isomers of the $Pt_6 - Pt_9$ clusters in this article, this diagram is complete for this size range. All relations of 17 different locally stable structures of the Pt_9 have

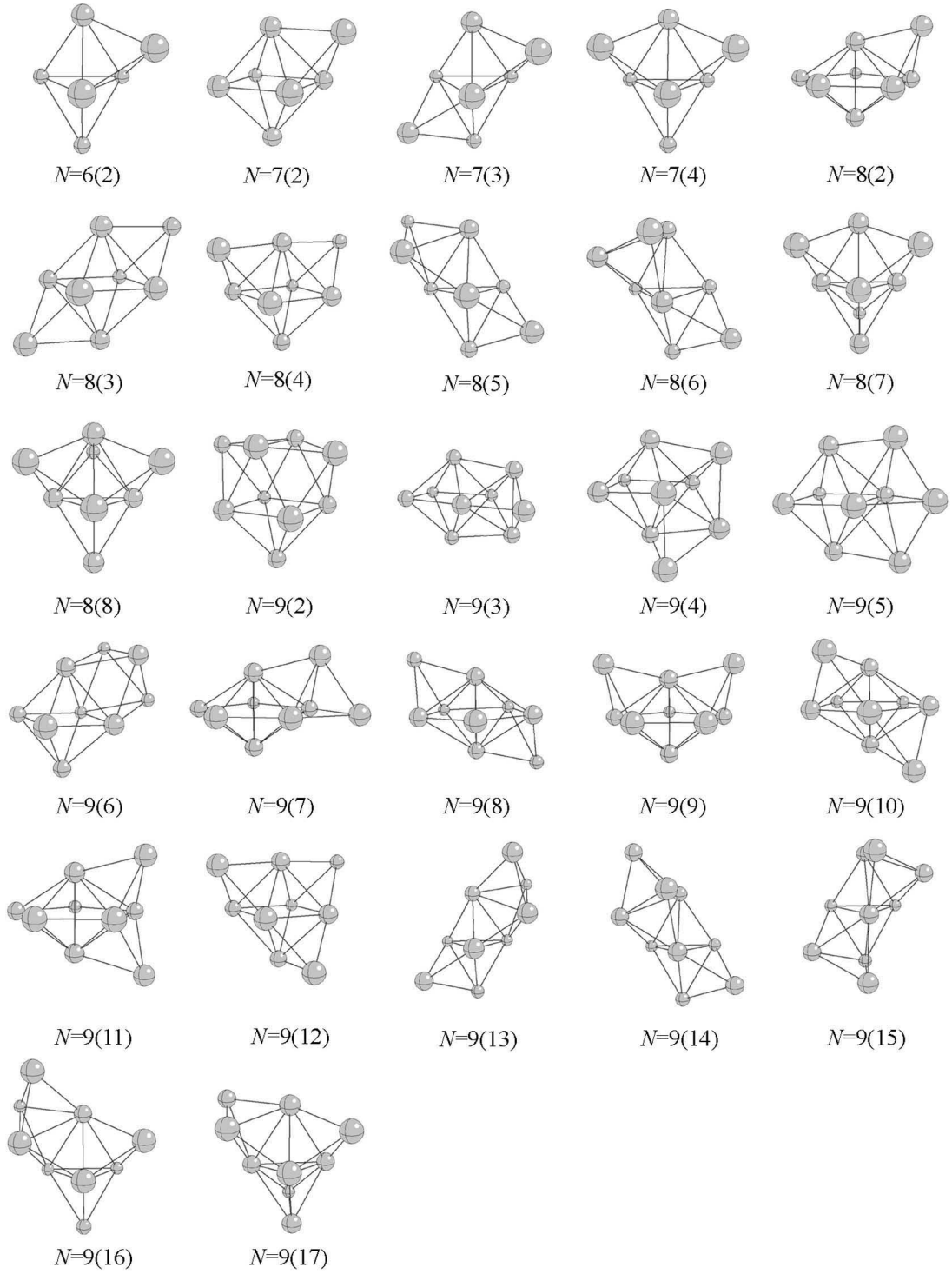


Figure III.4: All locally stable structures of $Pt_6 - Pt_9$ clusters other than the global minima

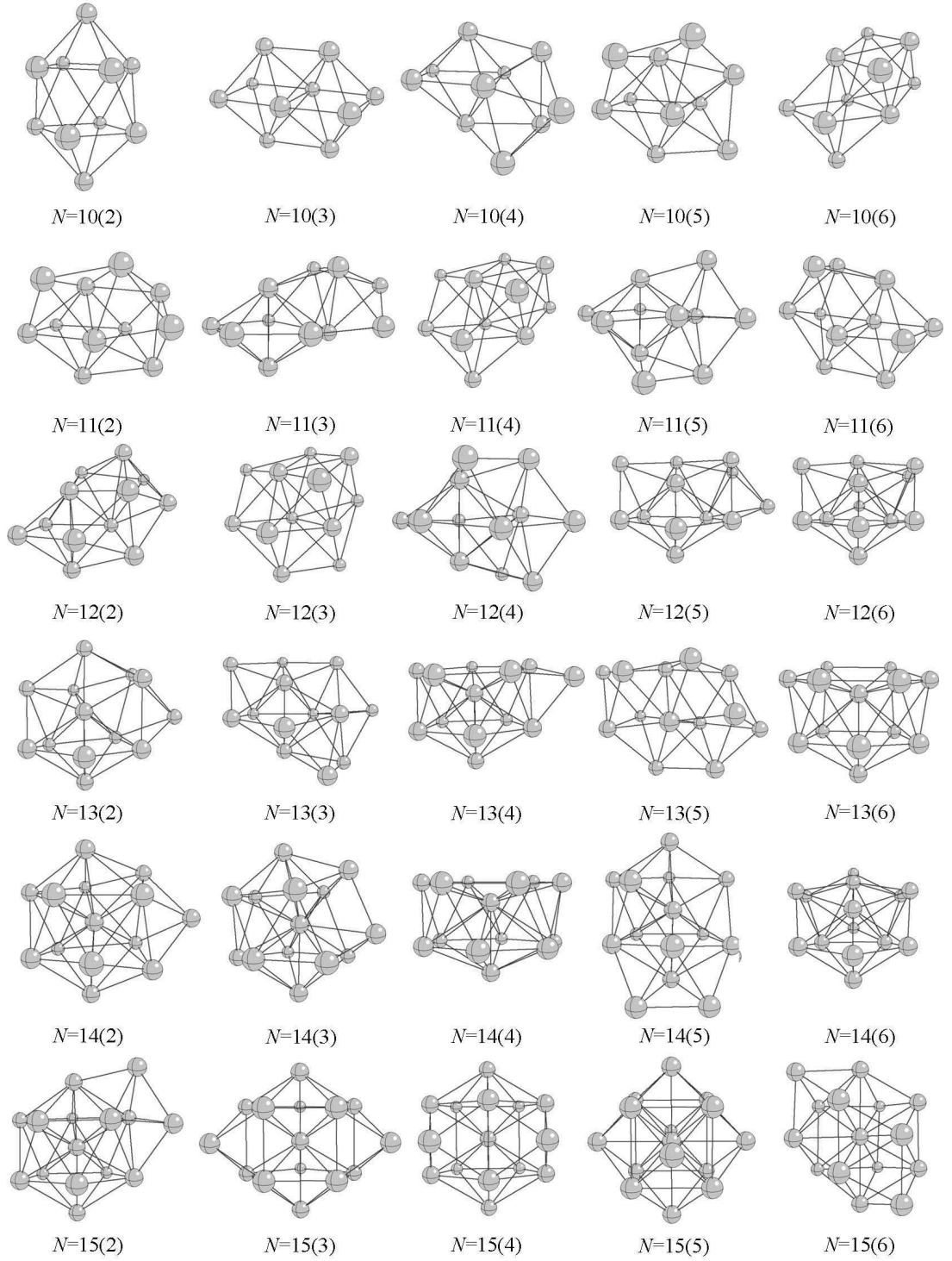


Figure III.5: The $2^{nd} - 6^{th}$ locally stable structures of the $Pt_{10} - Pt_{15}$ clusters

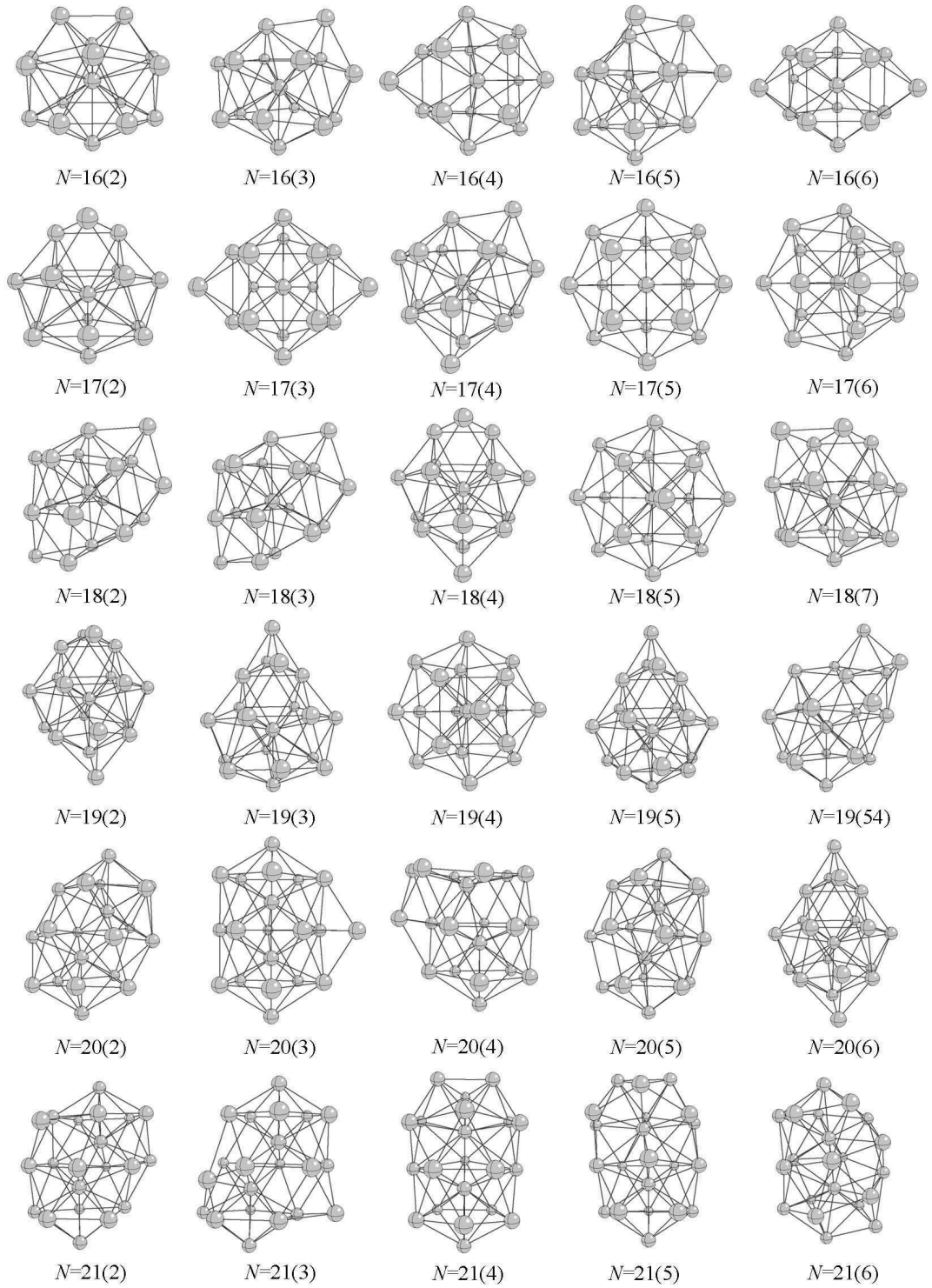


Figure III.6: Some locally stable structures of $Pt_{16} - Pt_{21}$ clusters

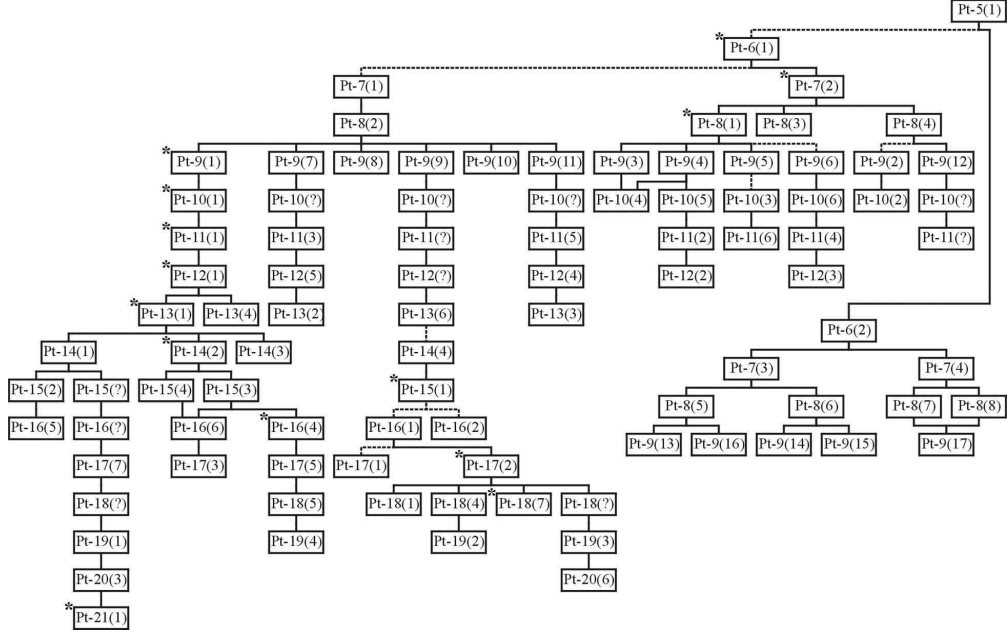


Figure III.7: Growth pattern of the locally stable structures of small Pt clusters. * denotes the most probable isomers

been shown in the diagram. But for the remaining parts, we have placed only many of those geometries that we have given in Fig. III.5, and Fig. III.6. They may have some other relations than the ones shown in the figure. Nevertheless, the diagram shows that there are some simple growth paths such as $Pt_5(1)$ - $Pt_6(2)$ - $Pt_7(3)$ - $Pt_8(5)$ - $Pt_9(13)$, or $Pt_6(1)$ - $Pt_7(2)$ - $Pt_8(3)$, or $Pt_7(1)$ - $Pt_8(2)$ - $Pt_9(1)$ - $Pt_{10}(1)$ - $Pt_{12}(1)$ - $Pt_{13}(1)$ - $Pt_{14}(1)$ - $Pt_{15}(2)$ - $Pt_{16}(5)$ in which each structure is related to the previous structure by type one. Simple growth paths can be considered in the formation of Pt clusters under the experimental conditions (near room temperature). For instance, when a $Pt_5(1)$ cluster meets a free Pt atom at room temperature, we expect that they form the structure of the $Pt_6(2)$ first. Because of the large potential energy difference between the $Pt_5(1)$ and the $Pt_6(2)$, the $Pt_6(2)$ melts as it forms. Due to the cooling process it loses its internal kinetic energy, and eventually it "falls" into the basin of

Table III.2: Total energies (eV) for all isomers of $Pt_6 - Pt_8$ and for the first 8 isomers of $Pt_9 - Pt_{21}$

N	$N(1)$	$N(2)$	$N(3)$	$N(4)$	$N(5)$	$N(6)$	$N(7)$	$N(8)$
6	-22.435	-21.788						
7	-27.219	-26.811	-26.249	-26.198				
8	-31.888	-31.532	31.189	-31.097	-30.717	-30.652	-30.563	-30.476
9	-36.709	-36.574	-36.178	-36.171	-36.137	-36.130	-35.908	-35.845
10	-41.646	-41.248	-41.208	-41.182	-41.180	-41.141	-41.017	-40.998
11	-46.462	-46.162	-46.097	-46.093	-45.949	-45.896	-45.883	-45.846
12	-51.609	-51.080	-50.972	-50.942	-50.909	-50.909	-50.855	-50.760
13	-57.583	-55.968	-55.906	-55.868	-55.825	-55.815	-55.795	-55.793
14	-61.732	-61.617	-61.444	-61.272	-60.924	-60.863	-60.810	-60.790
15	-66.951	-66.785	-66.401	-66.362	-66.073	-66.061	-65.951	-65.908
16	-71.861	-71.827	-71.807	-71.755	-71.690	-71.439	-71.397	-71.303
17	-76.830	-76.824	-76.787	-76.775	-76.770	-76.724	-76.641	-76.537
18	-81.696	-81.686	-81.683	-81.658	-81.647	-81.635	-81.582	-81.569
19	-86.922	-86.527	-86.503	-86.503	-86.493	-86.482	-86.461	-86.424
20	-91.729	-91.723	-91.640	-91.473	-91.440	-91.381	-91.319	-91.286
21	-96.829	-96.642	-96.629	-96.610	-96.609	-96.600	-96.594	-96.528

attraction of the $Pt_6(1)$. If both locally stable structures of the Pt_6 clusters near room temperatures interchange one to another, then they may both exist under the experimental condition. Similar processes may occur in the formation of the locally stable structures of the other sizes under the experimental conditions. The total energies calculated for all isomers of the $Pt_6 - Pt_8$ and for the first 10 isomers of the $Pt_9 - Pt_{21}$ are given in Table III.2. The differences between the total binding energies of any successive sizes are at least on the order of eVs. This quantity decreases to deVs for the successive isomers of a given size, if their backbones are different. For instance, the energy difference between $Pt_6(1)$ and $Pt_6(2)$ is 0.647 eV, or it is 0.562 eV between $Pt_7(2)$ and $Pt_7(3)$. An exception of this is that the energy difference between $Pt_{13}(1)$ and $Pt_{13}(2)$ is 1.615 eV, which is very high because of the highly symmetric structure of $Pt_{13}(1)$. If the backbones of the successive isomers are the same,

their energy difference is even on the order of eVs. For example, the energy gap between $Pt_7(3)$ and $Pt_7(4)$ is only 0.051 eV.

III.4 Probabilities

Probability of sampling different basins of attractions has been calculated by dividing the number of clusters in the basins by the total number of initial configurations. We have given these probabilities for all isomers of the Pt_6-Pt_8 and the first 9 isomers of the $Pt_9 - Pt_{21}$ in Table III.3. All probabilities given in Table III.3 have been obtained by quenching the high temperature (about 2600 K) initial configurations. The total energies of these samples effect the probability of getting the various isomers, in principle. In order to analyze this effect, we have performed some calculations on the sampling probabilities of the Pt_9 clusters with different total energies, i.e., at different temperatures. The probabilities of forming the various isomers of the Pt_9 clusters obtained by quenching 1900 K, 2600 K, 3000 K, 3500 K, and 4000 Ks have been given in Table III.4. Except for the case of 1900 K, the same number (17) of isomers has been obtained. Thus, 2600 K is high enough to sample the total number of locally stable structures. As the total energies of the clusters increase, the sampling probabilities of the first two isomers are decreasing, whereas those of the isomers with higher energies increase. This situation might be explained as the following: In our calculations, we prepared 10,000 initial configurations by recording their coordinates at each 500 steps of the MD trajectory. When the internal kinetic energies of the particles are relatively small, they cannot

Table III.3: Probabilities of all isomers of $Pt_6 - Pt_8$ and the first 9 isomers of $Pt_9 - Pt_{21}$

N	$N(1)$	$N(2)$	$N(3)$	$N(4)$	$N(5)$	$N(6)$	$N(7)$	$N(8)$	$N(9)$
6	0.568 ^a	0.432							
7	0.423	0.445 ^a	0.111	0.022					
8	0.552 ^a	0.375	0.018	0.036	0.007	0.008	0.003	0.000	
9	0.357 ^a	0.164	0.153	0.117	0.081	0.010	0.033	0.031	0.025
10	0.244 ^a	0.055	0.049	0.182	0.164	0.049	0.059	0.011	0.068
11	0.252 ^a	0.224	0.069	0.047	0.033	0.104	0.060	0.026	0.048
12	0.188 ^a	0.159	0.011	0.006	0.033	0.057	0.095	0.056	0.034
13	0.821 ^a	0.055	0.005	0.012	0.008	0.014	0.000	0.008	0.002
14	0.092	0.532 ^a	0.005	0.052	0.021	0.004	0.018	0.009	0.005
15	0.673 ^a	0.115	0.032	0.004	0.002	0.022	0.007	0.009	0.003
16	0.166	0.027	0.217	0.268 ^a	0.097	0.013	0.006	0.001	0.008
17	0.024	0.283 ^a	0.029	0.076	0.014	0.009	0.050	0.090	0.008
18	0.016	0.025	0.015	0.097	0.008	0.011	0.157 ^a	0.038	0.041
19 ^b	0.023	0.008	0.010	0.001	0.013	0.007	0.039	0.009	0.019
20	0.016	0.117 ^a	0.006	0.024	0.003	0.004	0.001	0.002	0.004
21	0.230 ^a	0.018	0.001	0.046	0.083	0.016	0.013	0.001	0.005

^aThe most probable isomer

^b0.040 is the highest probability belonging to the 54th isomer

Table III.4: The probabilities of sampling the isomers of Pt_9 clusters obtained by quenching 1900 K, 2600 K, 3000 K, 3500 K, and 4000 K initial configurations

Isomer number	1900 K	2600 K	3000 K	3500 K	4000 K
$N(1)$	0.496	0.367	0.329	0.299	0.278
$N(2)$	0.207	0.164	0.143	0.108	0.101
$N(3)$	0.104	0.153	0.181	0.199	0.201
$N(4)$	0.062	0.117	0.131	0.144	0.153
$N(5)$	0.066	0.081	0.073	0.071	0.076
$N(6)$	0.008	0.010	0.012	0.014	0.013
$N(7)$	0.019	0.033	0.033	0.048	0.047
$N(8)$	0.017	0.031	0.037	0.036	0.042
$N(9)$	0.010	0.025	0.028	0.034	0.036
$N(10)$	0.009	0.020	0.018	0.022	0.024
$N(11)$	0.002	0.004	0.006	0.006	0.009
$N(12)$		0.002	0.002	0.003	0.003
$N(13)$		0.001	0.002	0.004	0.006
$N(14)$		0.002	0.003	0.006	0.007
$N(15)$		0.000	0.002	0.002	0.002
$N(16)$		0.001	0.001	0.003	0.003
$N(17)$		0.000	0.000	0.001	0.001

go far away in a limited number of time steps (500) in the phase space from the starting point. Since the most stable isomers, in general, occupy larger potential "wells" in the phase space, sampling at relatively lower temperatures will favor these lowest energy structures. On the other hand, the clusters with higher internal kinetic energies can travel longer distances in a given time in the phase space. Therefore, a larger number of the initial configurations can escape from the lowest energy potential "wells" at higher temperatures. Thus, energetically higher basins of attractions in PES are visited more at higher temperatures compared to the cases of the samplings at relatively lower temperatures. Nevertheless, the quantitative changes in probabilities from 2600 K to 4000 K are not big enough to change the trend of the probability distribution. Namely, even at 4000 K, the lowest energy structure is still the most probable one, the probabilities still decrease as the energies of the isomers increase, and the order of the isomers with respect to their probabilities do not change drastically. These results also indicate that higher potential "wells", in general, occupy smaller volumes in the phase space. Therefore, the data given in Table III.3 might be used to investigate the trend of the isomer sampling probability distributions of small Pt clusters. Here, it should also be mentioned that for the larger clusters ($N \geq 20$), temperatures higher than 2600 K might be required in order to sample all stable isomers.

The probability distributions of the $Pt_6 - Pt_{13}$, and $Pt_{14} - Pt_{21}$ clusters obtained by quenching 2600 K clusters are given in Figs. III.8 and III.9, respectively. The probability of getting a specific isomer of a given size highly

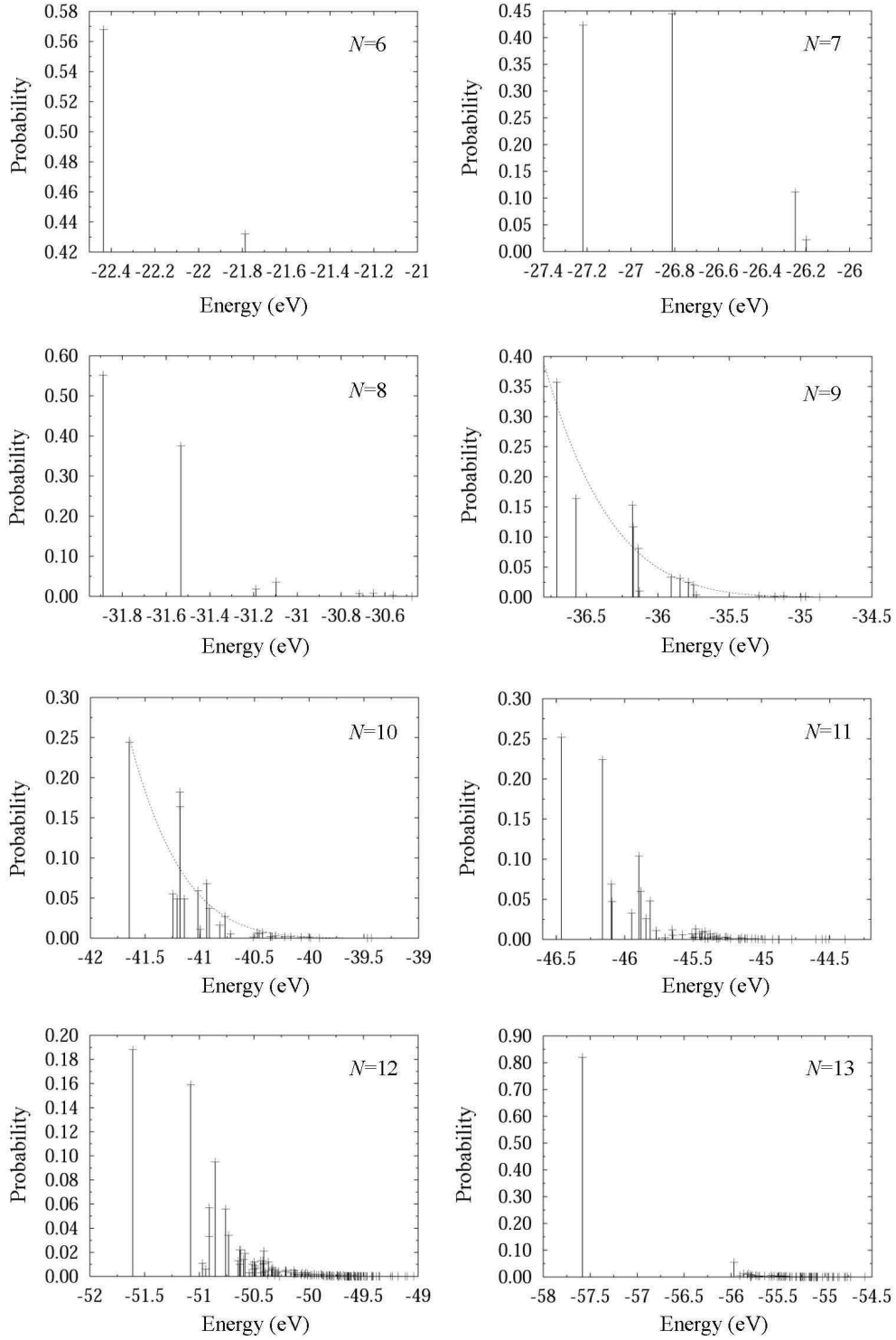


Figure III.8: The probability distributions of the isomers of $Pt_6 - Pt_{13}$ clusters obtained by quenching 2600 K initial configurations

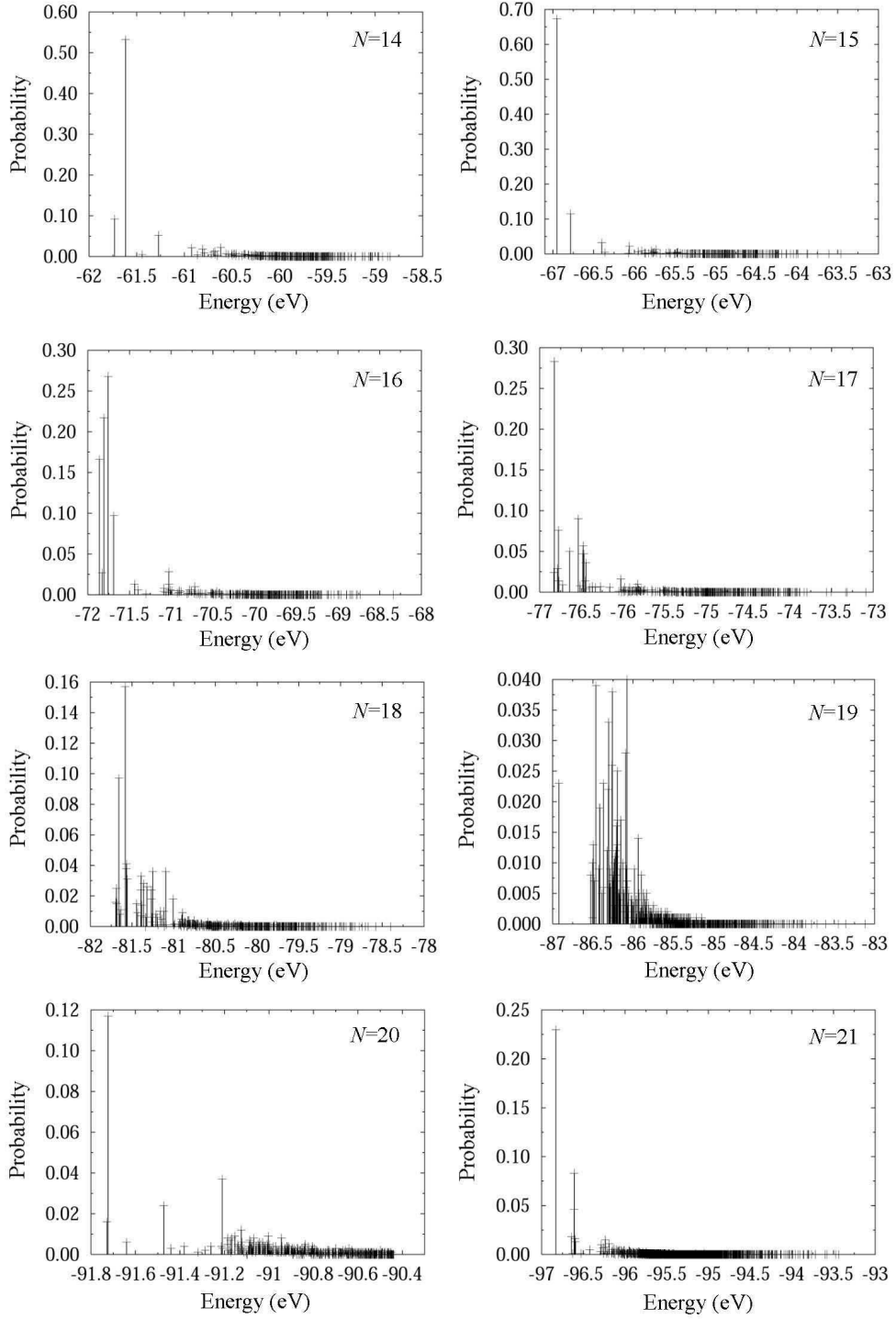


Figure III.9: The probability distributions of the isomers of Pt_{14} – Pt_{21} clusters obtained by quenching 2600 K initial configurations

depends on the energy of the isomer. A common characteristic of all distributions is that, as the total energies of the isomers increase, the probabilities decrease. One can fit the most of the probabilities in a distribution of a given size using the form

$$P(E) = a \exp\left(\frac{b}{E + c}\right) \quad (\text{III.3})$$

where, $a > 0$: the dimensionless constant, $b > 0$: scaling factor in units of eV, $0 < c < |E_h|$ (E_h is the energy of the energetically highest isomer), and $E < 0$ is the internal energy of a quenched isomer [65, 66] (see the probability distribution graphs of Pt_9 and Pt_{10} in Fig. III.8). Thus, for many cluster sizes, the most stable structure is the most probable one. However, there are some exceptions, e.g., $Pt_7(2)$, $Pt_{14}(2)$, $Pt_{16}(4)$, $Pt_{17}(2)$, $Pt_{18}(7)$, $Pt_{19}(54)$, and $Pt_{20}(2)$ which are more probable than their least energy structures. Similarly, some isomers have higher probabilities than their less energetic neighbors. For example, the probability of the $Pt_{10}(4)$ is higher than the probabilities of the $Pt_{10}(2)$ and $Pt_{10}(3)$. This means that the energy is not the only control parameter. The secondary parameters affecting the probabilities are the simple growth path, the number of accessibility from the structure of the previous size, the backbone and the symmetry of the cluster. The probability of formation of $Pt_7(2)$ can be given as an example of the effect of the simple growth path. Although the total energy of $Pt_7(1)$ is less than that of $Pt_7(2)$, sampling probability of the $Pt_7(2)$ is higher than that of the $Pt_7(1)$. This is due to the fact that $Pt_7(2)$ is connected to their common parent $Pt_6(1)$ by type 1, whereas $Pt_7(1)$ is connected by type 2. Namely, $Pt_7(2)$ is on the simple growth

path $Pt_6(1)$ - $Pt_7(2)$, but $Pt_7(1)$ is not. A similar thing occurs at size $N=17$. Since $Pt_{17}(2)$ is on the simple growth path i.e., $Pt_{16}(1)$ - $Pt_{17}(2)$, its sampling probability is higher than that of $Pt_{17}(1)$. It should be noted that the effect of being on a simple growth path may not overcome always the effect of energy as seen on the example of $Pt_5(1)$ - $Pt_6(2)$. Although $Pt_6(2)$ is on the simple growth path, the sampling probability of the $Pt_6(1)$ is higher than that of the $Pt_6(2)$, since the energy difference is large between them (0.65 eV).

The effect of the number of accessibility from the structure of the previous size can be seen in the sampling probability differences of the $Pt_8(3)$ and the $Pt_8(4)$. Although the total energy of the $Pt_8(3)$ is lower than that of the $Pt_8(4)$, and both of them are connected to a common parent $Pt_7(2)$ by type 1, the probability of formation of the $Pt_8(4)$ is twice of that of the $Pt_8(3)$. This can be explained by the fact that the structure of the $Pt_8(3)$ can be obtained from the structure of the $Pt_7(2)$ in a single way: by adding the last atom to cap the symmetric face of the $Pt_7(2)$ with respect to the center of the tetragonal bipyramid (see Fig. III.4). On the other hand, structure of the $Pt_8(4)$ can be obtained from the structure of $Pt_7(2)$ in three ways: by capping one of the appropriate three faces of the tetragonal bipyramid. A similar situation can be found in the sampling probabilities of the $Pt_{14}(1)$ and the $Pt_{14}(2)$ clusters.

Effect of the backbone on the sampling probability is visible for the $Pt_9(6)$ and the $Pt_9(7)$ isomers. Generally, as the total energy of the locally stable structures increases, the backbones of the structures change from the hexagonal, pentagonal, tetragonal to trigonal bipyramids. Sometimes this order is

broken as in the case of the pass from the $Pt_9(6)$ to the $Pt_9(7)$. The backbone of the $Pt_9(6)$ is a tetragonal bipyramid but that of the $Pt_9(7)$ - $Pt_9(10)$ are pentagonal bipyramids. Thus, the sampling probability of the $Pt_9(7)$ - $Pt_9(10)$ are higher than that of the $Pt_9(6)$. The backbones are also responsible for the energy bands and energy gaps in many of the probability distribution graphs. There are some energy bands in which a number of energetically close isomers with smoothly decreasing probabilities are present, and there are some energy gaps in which there are no isomers. Generally, after an energy gap the probability drops drastically as in the case of the $Pt_9(3-6)$ and the $Pt_9(7-11)$ isomers. This is due to the fact that their backbones are different, and also probability of sampling is a function of the isomer's energy (Eq. III.3).

Finally, the effect of the symmetry is best seen in the size of $N=13$. The probability distribution graph of the Pt_{13} differs from the others, noticeably. In this size, the probability of the lowest energy structure is much higher than those of the other isomers because of the perfect spherical symmetry of the icosahedron. On the other hand, however, the probability distribution of the Pt_{19} shows that there are many other isomers having approximately equal probabilities to that of the $Pt_{19}(1)$ (one may have to use much larger sampling size of the initial conditions for larger sizes in order to have converged probabilities).

We denote the highest probable isomers in Fig. III.7 by an asterisk. It is not surprising that many of them ($Pt_9(1)$ - $Pt_{10}(1)$ - $Pt_{11}(1)$ - $Pt_{12}(1)$ - $Pt_{13}(1)$ - $Pt_{14}(2)$) are on the same simple growth path. On the other hand, the structures such

as $Pt_9(6)$, $Pt_{10}(3)$, $Pt_{16}(1)$, $Pt_{16}(2)$, $Pt_{17}(1)$, and $Pt_{20}(1)$, which are connected to their parents by type 2, have relatively low probabilities with respect to the probabilities of their neighbors.

It should be noted that probabilities of formation given here belong to the structures which are stable at 0 K. Many of these geometries may not be stable at room temperatures, i.e., potential wells may be very shallow. Therefore, to find the most probable structure in the experimental conditions, one should check the stability of these structures at room temperatures. The temperature could also be a factor that would influence the path from one cluster to the other. The stability of the structures as a function of temperature and the influence of temperature on the growth paths can be discussed in detail in the future works.

CHAPTER IV

$Pt_{22} - Pt_{56}$ CLUSTERS

IV.1 Computational Details

The search of the global minima of the larger sizes ($N \geq 22$) has been done in two phases. In the first phase, initially 500 independent configurations prepared along high-energy trajectories (about 2600 K) have been quenched to obtain a first candidate for the global minimum structure for each size of the clusters (in this size range we limit the number of independent initial conditions to 500 since further steps of the search are highly computationally demanding). After that, internal kinetic energies of these first candidates of the global minima have been increased in a stepwise manner and their short-time average internal kinetic energies (STKE) are monitored as a function of time at different total energies. Any transition from one of the basins of attraction to another one affects the internal kinetic energy. Therefore, any phase change can be detected as an abrupt change in STKE as shown in Fig. IV.1. When

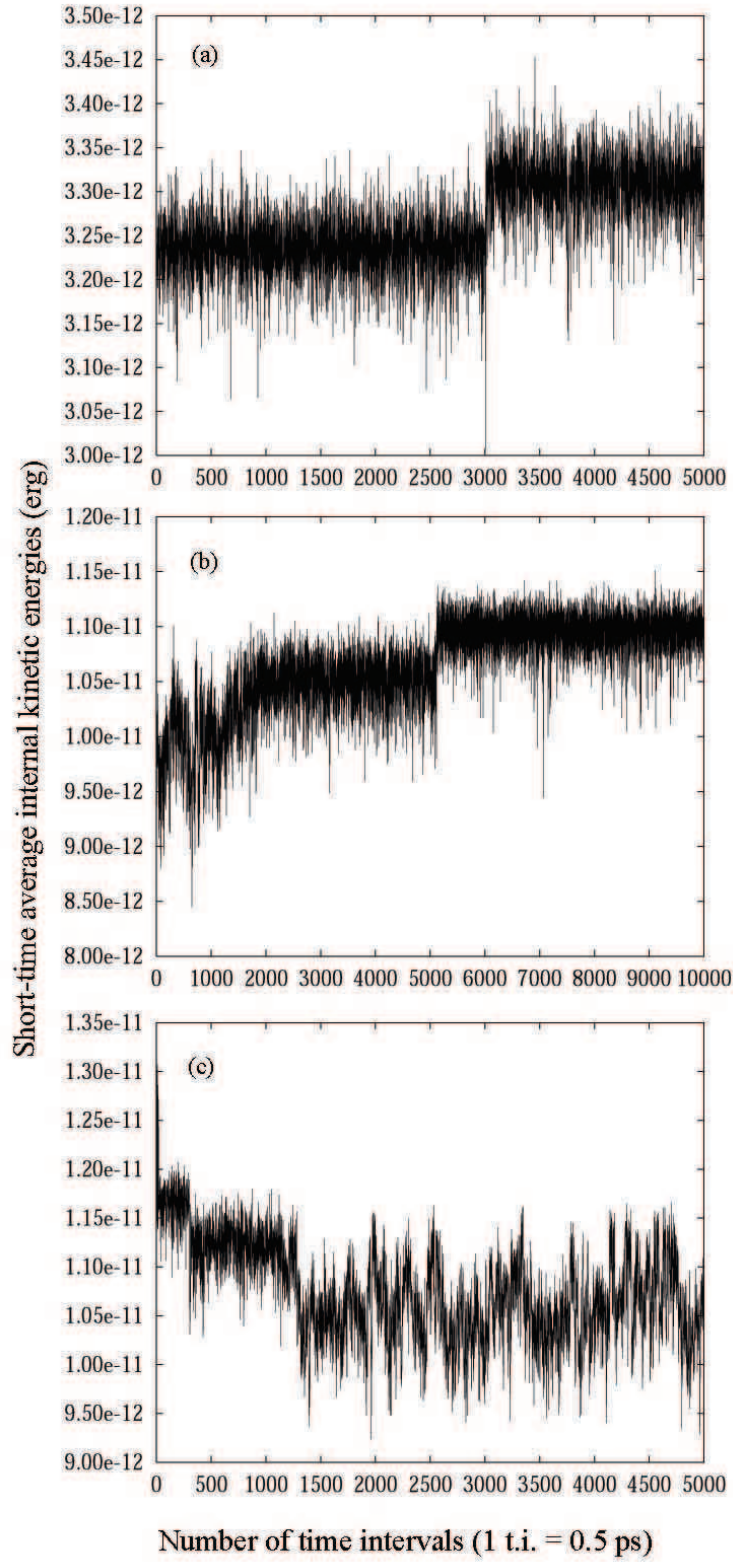


Figure IV.1: The short-time average internal kinetic energies versus time graphs of Pt_{55} clusters (a) for the first candidate at 297 K, (b) for the second candidate at 969 K, (c) for the global minimum structure at 979 K

the total energy is high enough to pass over the barrier between the basins, clusters change their basins of attraction. If there is a lower energetic locally stable structure near the current basin of attraction of the cluster, that lower energetic basin of attraction biases the motion of the atoms in the phase space towards itself. Thus, whenever a jump to a higher STKE is observed, this new energetically lower isomer is considered as the second candidate for the global minimum structure and it is quenched and then heated gradually again. By repeating these quenching, heating, and monitoring processes we have searched a descending sequence of local minima for each size. The STKE of Pt_{55} clusters for the first, second candidates and that of the global minimum structure are given in Fig. IV.1(a), (b) and (c), respectively. In Fig. IV.1(a) and (b) there are jumps indicating the changes of the current basins of attraction to the neighboring lower energetic basins of attraction. However, the STKE of the global minimum structure of Pt_{55} cluster given in Fig. IV.1(c) never climbs over its initial kinetic energy during the same amount of observation time. Instead, it starts to visit the neighboring higher energetic basins of attraction. The method of the successive quenching and reheating MD phases described here is used before for Pd clusters by Karabacak et al. [67] and for Cu clusters by Özçelik and Güvenç [68].

A descending sequence of local minima terminates at a distinguished potential well from which no further descent is possible. This bottom structure is the lowest-energy structure of that "funnel". However, there may be more than one "funnel" in a potential energy surface (PES) [69]. Namely, the de-

scending sequences of local minima started from different initial configurations can terminate at different bottom structures. Different "funnels" are related to different structural morphologies. If the correct "funnel" is missed in the preparation of the 500 initial configurations, the real global minima may not be caught by the described procedure. Since as it is phrased by Wales and Doye [40] that "The most obvious short-cut would be to start not from initial random configurations but from seeds with either decahedral, icosahedral or fcc morphologies", in order to investigate the other possible "funnels" which may possess the global minimum structure, we performed the second phase of our calculations in which two things have been done: 1. We have compared our results with the Monte Carlo minimization (or basin-hopping algorithm) study carried out using Sutton-Chen (SC) potentials by Doye and Wales [53]. We found that their 37-, 38-, 42-, 44-, and 50-atom structures have lower potential energies than our initial results. Therefore, we repeat the first phase of our calculations for these sizes by starting from the structures reported in Ref. [53]. Another study of *Pt*, *Pd* and *Pt - Pd* bimetallic clusters, with up to 56 atoms, performed by Johnston and co-workers [55] can also be considered for the comparison. Johnston and co-workers have reported the global minima for the mentioned clusters using the many-body Gupta potential in their genetic algorithm calculations. Since the most of their structures are very similar to those found by Doye and Wales, we have been contented with the first comparison. 2. Whenever the morphology of the global minimum structure of a size N is different from the morphology of the neighboring sizes,

$N - 1$ and/or $N + 1$, we have examined structure of the size N in the form of neighboring size morphology. By this second consideration we have found lower energetic structures for 51-, 53-, and 54-atom clusters. Finally, we have applied the same heating, monitoring and quenching procedure to these new 8 structures ($N=37, 38, 42, 44, 50, 51, 53$, and 54) once more. In only STKE of the 44-atom structure we observed a small jump at about 650 K. After quenching this new lower energetic structure, we obtained the final putative global minimum structure of this size.

Most of the failures in the investigation of the global minima in the first phase of our calculations are due to the topographies of the potential energy surfaces (PES) which are likely to have multiple "funnels" in these 8 sizes [70] and due to computationally limited search time. To emphasize how difficult to find the lowest energy structure in certain sizes, we perform the following extra calculations: We have added the L-BFGS conjugate gradient routine [71] to our MD program. Starting from a random initial configuration, we let the 38-atom *Pt* cluster take 10 million time steps in the phase space at about 2700 K. After each MD step, the L-BFGS subroutine is performed to relax the cluster into the nearest local minima, by minimizing the cluster potential energy as a function of the cluster coordinates. In some cases the conjugate gradient subroutine could not perform the minimization process due to the errors in the numerical derivatives. Within the 8,596,259 successful minimization 127,510 different local minima were found. During the whole trip the basin of attraction of the lowest energy structure (truncated octahedron) was visited only 1012 times.

Therefore, if we had chosen randomly 10,000 (nearly equal to 10 million / 1012) sets of configurations among 10 million sets produced in the MD trajectory and if we had used them as our initial configurations in the first phase of our calculations, only one of them would have ended up with the global minimum structure, on average. We discuss the morphologies of the global minima in the next section. After all of these considerations, still we cannot be sure that we obtained the real global minima, which is the case for any other global optimization method too. Nevertheless, the structures presented here can be considered, at least, as good starting points for further investigations and illuminate the growth path of the clusters.

IV.2 Global Minima

We have reported the total energies (E), energies per particle (E/N), the point groups (PG), the structural assignments (SA), the average bond lengths (R_b) and the differences between the maximum and minimum bond lengths (D_R) of all the global minima in Table IV.1. The point groups of the structures are determined with the help of a program taken from OPTIM program [72]. Symmetry elements are diagnosed when rotation and reflection operators produce the same geometry correct to 0.01 in each Cartesian coordinates. We have also indicated the global minima in Table IV.1 if they are common with SC *Pt* clusters reported in Ref. [53]. The energies and the second finite differences in energies (D_2E) are plotted in Fig.IV.2(a) and (b), respectively. For the sake of completeness we have included the energies of the sizes $N=2-21$

Table IV.1: Results for global minima of $Pt_{22} - Pt_{56}$ clusters

N^a	E^b	E/N^c	PG^d	SA^e	R_b^f	D_R^g
22	-102.088	-4.640	C_1	face-sharing icosahedral	2.642	0.520
23	-107.231	-4.662	C_2	face-sharing icosahedral ^h	2.650	0.572
24	-112.161	-4.673	C_s	face-sharing icosahedral ^h	2.630	0.325
25	-117.011	-4.680	C_3	face-sharing icosahedral	2.664	0.606
26	-122.241	-4.702	C_1	face-sharing icosahedral	2.659	0.633
27	-127.459	-4.721	C_s	face-sharing icosahedral	2.662	0.591
28	-132.707	-4.740	C_s	face-sharing icosahedral	2.645	0.613
29	-137.741	-4.750	C_2	face-sharing icosahedral ^h	2.645	0.466
30	-143.039	-4.770	C_{3v}	face-sharing icosahedral ^h	2.650	0.370
31	-147.999	-4.774	C_3	face-sharing icosahedral	2.679	0.540
32	-153.179	-4.787	D_{2d}	face-sharing icosahedral	2.660	0.516
33	-158.230	-4.795	C_2	face-sharing icosahedral	2.659	0.514
34	-163.357	-4.801	C_s	face-sharing icosahedral	2.654	0.578
35	-168.730	-4.821	D_3	face-sharing icosahedral	2.668	0.529
36	-173.924	-4.831	C_{2v}	face-sharing icosahedral ^h	2.647	0.357
37	-179.068	-4.840	C_{2v}	decahedral ^h	2.677	0.343
38	-184.483	-4.855	O_h	truncated octahedron ^h	2.679	0.180
39	-189.486	-4.859	C_s	centred icosahedral	2.660	0.481
40	-194.816	-4.870	D_2	face-sharing icosahedral	2.670	0.439
41	-199.675	-4.870	C_1	centred icosahedral	2.661	0.552
42	-204.886	-4.878	C_s	centred icosahedral ^h	2.689	0.504
43	-210.185	-4.888	C_2	centred icosahedral	2.661	0.537
44	-215.526	-4.898	C_1	centred icosahedral	2.671	0.597
45	-220.694	-4.904	C_s	centred icosahedral ^h	2.657	0.490
46	-225.965	-4.912	C_s	centred icosahedral	2.672	0.529
47	-231.146	-4.918	C_1	centred icosahedral	2.674	0.615
48	-236.397	-4.925	C_1	centred icosahedral ^h	2.672	0.607
49	-241.724	-4.933	C_1	centred icosahedral	2.670	0.551
50	-246.830	-4.937	D_{3h}	truncated octahedral ^h	2.689	0.196
51	-251.890	-4.939	C_{2v}	uncentred icosahedral	2.663	0.212
52	-257.678	-4.955	C_{2v}	uncentred icosahedral	2.665	0.233
53	-263.386	-4.970	C_{5v}	uncentred icosahedral	2.667	0.238
54	-269.011	-4.982	I_h	uncentred icosahedron	2.670	0.202
55	-273.454	-4.972	I_h	centred icosahedron	2.686	0.183
56	-278.389	-4.971	C_s	uncentred icosahedral	2.671	0.501

^aSize^bEnergy (eV)^cEnergy per particle^dPoint group^eStructural assignment^fAverage bond length (Å)^gDifference between max. and min. bond lengths (Å)^hCommon with Sutton-Chen structures given in Ref. [53]

into these two graphs. Following Northby *et al.* [73] and Lee and Stein [74], the function,

$$E_0 = aN + bN^{2/3} + cN^{1/3} + d, \quad (\text{IV.1})$$

is fitted to the energies given in Table IV.1, and it is subtracted from the energies of the clusters in order to emphasize the size dependence. In this polynomial function, a describes the volume, b surface, c edge, and d the vertex contributions to the energy. D_2E is generally correlated with the magic numbers observed in mass spectra. Clusters are particularly abundant at magic number sizes in mass spectra since they are the most stable ones [75].

The core, the surface and the triangulated polyhedral surface structures of $Pt_{22} - Pt_{39}$ global minima are illustrated in Fig.IV.3 and those of $Pt_{40} - Pt_{56}$ global minima are in Fig.IV.4. We call an atom in a cluster as a core-atom if its coordination number (CN), which is the number of nearest neighbors within a cutoff radius $1.2 r_e$, is greater than or equal to 10. The r_e (2.78 Å) is the nearest neighbor distance in the perfect crystal. The atoms with $5 \leq CN \leq 9$ are called as surface atoms and the atoms with $CN = 3 - 4$ are called as capping atoms. Definitions of the core and surface atoms given here are slightly different from those of Lee and co-workers [76]. They named the atoms with $CN = 10$ as surface atoms. The CN analysis of all the global minima is given in Table IV.2. In the Fig.IV.3 and Fig.IV.4, the bonds between the core and surface atoms are not presented to make the figures clearer. Furthermore, all the surface and the triangulated polyhedral structures are presented from the same points of view, whereas the figures of the structures which show explicitly

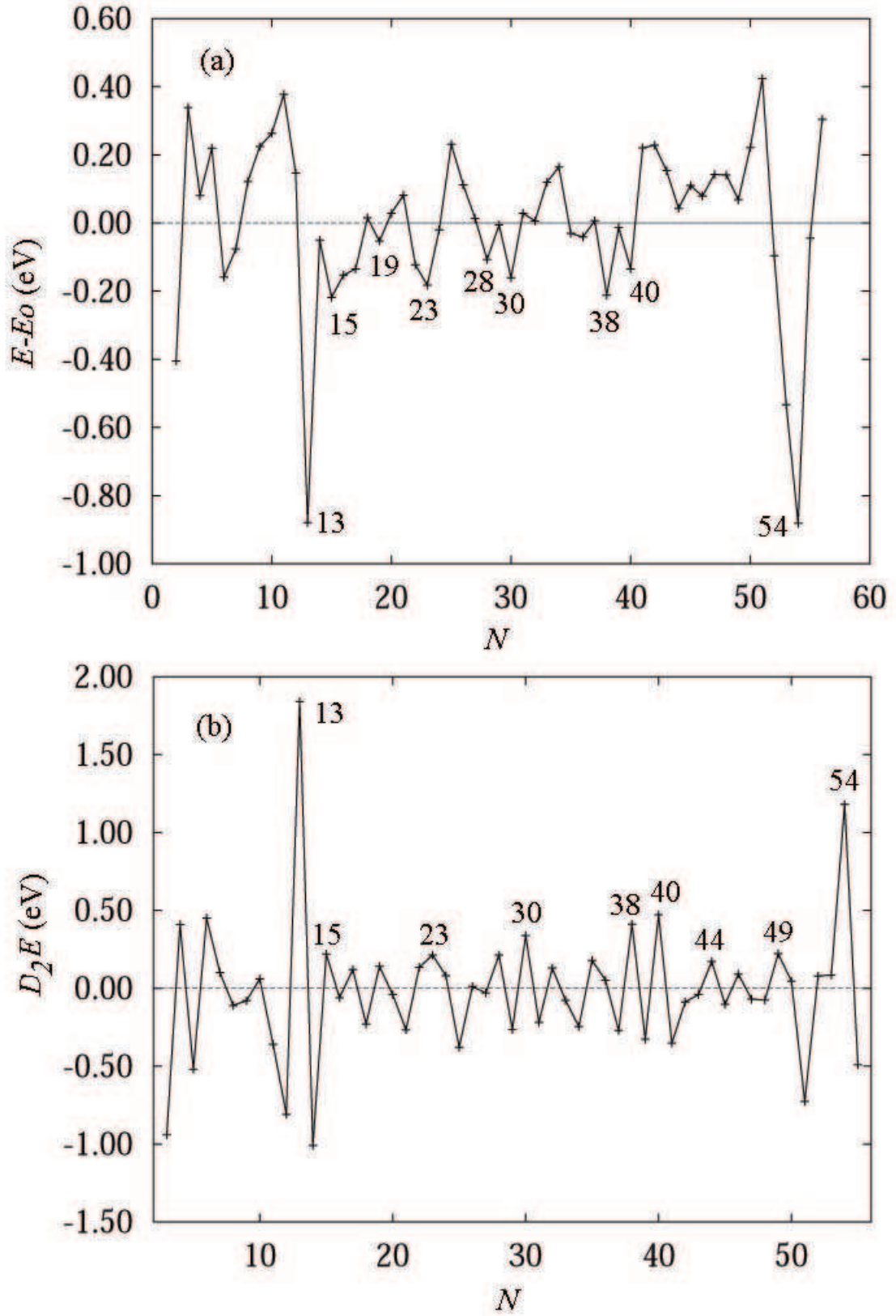


Figure IV.2: (a) Energies where $E_0 = 13.1113 - 11.2291N^{1/3} + 6.73356N^{2/3} - 6.20365N$ (b) The second finite difference in binding energy

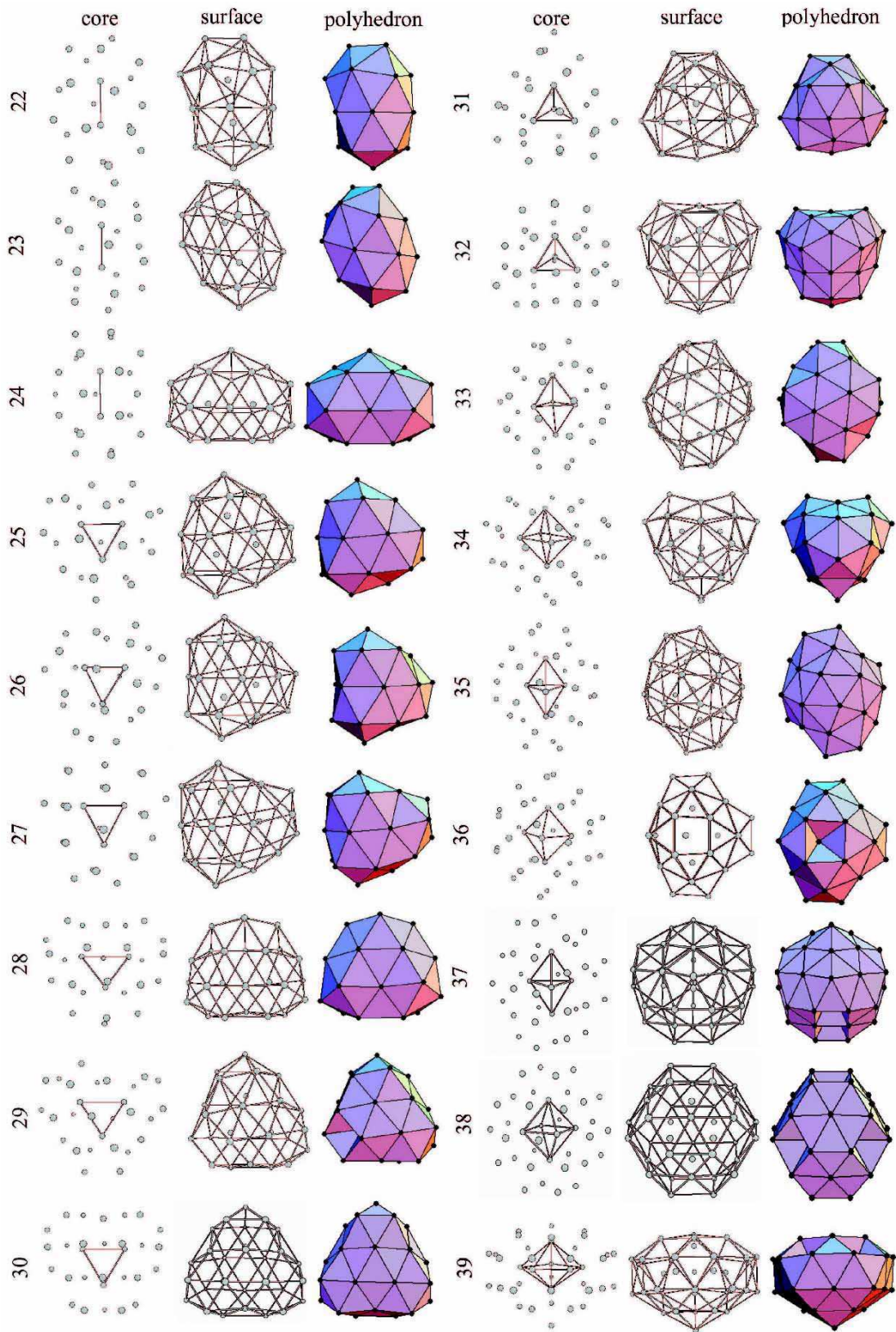


Figure IV.3: Global minima for $Pt_{22} - Pt_{39}$ clusters

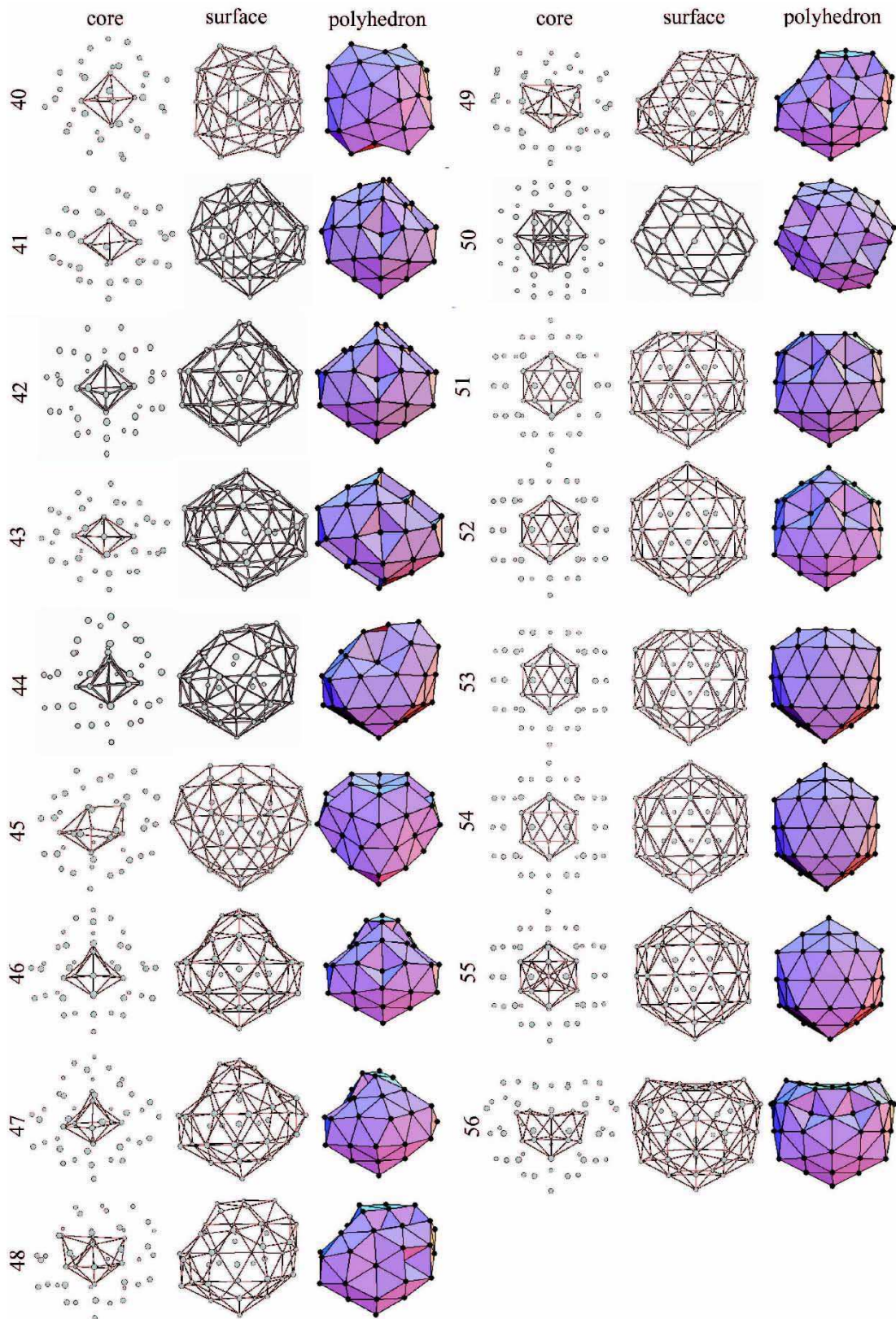


Figure IV.4: Global minima for $Pt_{40} - Pt_{56}$ clusters

the cores are rotated as a whole with respect to the remaining two figures by arbitrary angles to get the best view of the core part. From Fig.IV.2(a) it can be seen that the most stable structures occur at sizes 13 and 54. The 13-atom structure is a complete Mackay icosahedron [77] as we reported in our first paper [78], whereas the 54-atom structure is a Mackay icosahedron without a central atom. The icosahedral morphology without central atoms in the global minima of *Pt* clusters starts at the size of 51 and continues up to the size of 56 except the 55-atom structure which is a centred icosahedron. Since the icosahedral morphologies with and without a central atom have their own "funnels", we found only the 52- and 56-atom global minima at the end of the first phase of our calculations. Initially, the 51-, 53-, and 54-atom putative global minima had been found as some structures belonging to the centred icosahedral morphology. For instance, the 54-atom structure was a complete 55-atom icosahedron with missing one of the surface atoms among the ones having the least coordination number. After examining the uncentred icosahedral "funnel", we have found the global minima of these 3 sizes ($N=51$, 53 and 54). The energy difference between the 54-atom uncentred icosahedron and the 54-atom centred icosahedron with missing one surface atom is more than 1 eV. Although a central atom in an icosahedron has 12 *CN*, which is greater than the *CN* of any surface or capping atom, the uncentred 54-atom icosahedron has lower energy than the 54-atom icosahedron with a central atom. This is because of the fact that the central atom pushes the other atoms outwards and the spherical shells expand. The radius of the inner shell

Table IV.2: Coordination number analysis of $Pt_{22} - Pt_{56}$ clusters

Size	Coordination number									
N	5	6	7	8	9	10	11	12	13	14
22	0	13	5	2	0	0	0	1	1	0
23	0	12	6	3	0	0	0	0	2	0
24	1	14	5	2	0	0	0	0	2	0
25	0	12	3	6	1	0	0	3	0	0
26	0	13	4	5	1	0	0	2	1	0
27	0	13	4	7	0	0	1	0	1	1
28	1	12	8	4	0	0	1	0	2	0
29	2	12	6	6	0	0	0	1	2	0
30	0	12	9	6	0	0	0	0	3	0
31	0	12	6	6	3	0	0	1	3	0
32	0	12	12	0	4	0	0	4	0	0
33	2	10	8	8	0	1	0	4	0	0
34	1	13	10	4	0	2	1	3	0	0
35	0	12	6	12	0	0	0	5	0	0
36	0	16	6	9	0	0	4	1	0	0
37	2	18	2	10	0	0	0	5	0	0
38	0	24	0	0	8	0	0	6	0	0
39	0	15	7	10	0	0	3	4	0	0
40	0	12	8	14	0	0	0	6	0	0
41	1	17	5	10	2	0	0	4	2	0
42	2	18	1	14	0	0	0	4	3	0
43	0	18	6	12	0	0	2	3	2	0
44	0	15	8	12	1	1	0	5	1	1
45	2	14	6	15	0	2	4	2	0	0
46	0	16	6	14	2	0	1	4	3	0
47	0	14	7	17	1	0	1	6	1	0
48	0	18	5	15	0	2	1	3	4	0
49	0	17	4	18	0	1	3	5	1	0
50	0	24	6	0	8	3	0	9	0	0
51	0	12	9	18	0	3	9	0	0	0
52	0	11	8	21	0	2	10	0	0	0
53	0	11	5	25	0	1	11	0	0	0
54	0	12	0	30	0	0	12	0	0	0
55	0	12	0	30	0	0	0	13	0	0
56	0	15	7	21	2	0	7	4	0	0

of the 55-atom complete icosahedron is 2.6095 Å. The distance between the central atom and the surface atoms having 6 and 8 CN are 4.4653 Å and 5.1126 Å, respectively. However, the corresponding distances in the 54-atom uncentred icosahedron are 2.5207 Å, 4.4317 Å, and 5.0578 Å, which are all smaller. Another comparison can be made between the average bond lengths of the 54-atom structures having no central atom and missing one surface atom. The average bond length of the 54-atom global minimum structure (the uncentred icosahedron) is 0.015 Å less than that of the 54-atom centred icosahedron missing a surface atom.

Global minima of all the clusters from 51-atom to 54-atom have the same structure in their cores, i.e., a 12-atom uncentred icosahedron. The 12-atom uncentred icosahedron is stable at low temperatures but its energy is not lower than the global minimum structure of the 12-atom centred icosahedral cluster that we reported before [78]. The 12-atom uncentred icosahedron of gold cluster is reported as the global minimum structure by Wilson and Johnston [79] in their MD simulated annealing study carried out using an empirical Murrell-Mottram many-body potential function. Our uncentred icosahedral global minima of 51-, 52-, 53-, and 54-atom clusters are stable up to about 645 K, 803 K, 788 K, and 995 K, respectively. The energy of the uncentred icosahedral isomer of the 55-atom cluster, which has 6 atoms instead of 5 in one of the smaller rings on either pole of the uncentred icosahedron, is about 0.1 eV higher than that of the global minimum structure (55-atom centred icosahedron). The core of the global minimum structure of the 56-atom cluster is an

uncentred 12-atom icosahedron with a missing atom from the surface of the core.

From Fig.IV.2(a) it can be seen that the 54-atom uncentred icosahedron is more stable than the 55-atom centred icosahedron because its relative energy with respect to the reference energy E_0 is much lower than that of the 55-atom structure. Similarly, Fig.IV.2(b) shows that intensity of the 54-atom clusters in a mass spectrum should be much higher than that of the 55-atom clusters. However, one should note that the experimental conditions range from rapid cooling (mostly kinetic control) to long periods of heat treatment (mostly thermodynamic control) [80]. Since the global minima of the most of the smaller clusters have centred icosahedral morphology, as the *Pt* atoms aggregate in the laboratory conditions to form higher sizes, the structures having a central atom would be observed initially. It could take a relatively long time for a central atom to escape to the surface of the structure even if it has enough energy. Therefore, under kinetically controlled conditions, one would expect to find that the 55-atom centered icosahedron is more favorable in the mass spectra. On the other hand, if the experiments are mostly thermodynamic control in nature the global minimum structures should be observed, therefore, we would expect to find similar results to the ones that we report here in such conditions. Unfortunately we cannot find any experimental study on the structures or mass spectra of bare *Pt* clusters in the size regime considered here except the one performed by Andersson and Rosen [81]. They have reported the mass spectra of both bare *Pt* clusters and of the *Pt* clusters with adsorbed hydrogen

(deuterium) and oxygen molecules with clusters in the size range between 7- and 30-atoms. However, they haven't observed any size effect in their mass spectra of the bare *Pt* clusters (in the size range of 10-16) which does not correlate well not only with our D_2E given in Fig.IV.2(b) but also corresponding second difference in binding energy calculations of both Doye and Wales [53] and of Johnston and co-workers [55]. There are some experimental studies on the structures of *Ni* clusters by Riley and co-workers [82, 83, 84, 85]. Using nitrogen probe molecules, they have reported the global minimum structures of the 38- and 55-atom *Ni* clusters as truncated octahedron [84] and centred icosahedron [85], respectively, which are similar to our results for the corresponding *Pt* clusters. We could not find any experimental evidence for the 54-atom uncentred icosahedral structure of the metal clusters among the existing experimental studies, therefore, we believe that it should be taken into consideration and studied under proper conditions. We are also aware of the fact that at present it is often not possible to determine the structures of clusters unambiguously in the gas phase or in a molecular beam [6].

There are some shallow minima in the energy plot Fig.IV.2(a) at $N=15$, 19, 23, 28, 30, 38, and 40. We have reported before [78] the 15- and 19-atom global minima as a hexagonal bipyramid and a double icosahedron, respectively. The 23- and 30-atom global minima are common with SC gold and platinum clusters. The 23-atom structure resembles the 23-atom SC silver and rhodium global minimum [53]. All of the 22-, 23- and 24-atom global minima have two atoms in their cores. These structures can be classified as two

distorted phase-sharing icosahedra. All of the clusters between the sizes $N=25$ and $N=30$ have three atoms in their cores. These structures may be called as three distorted phase-sharing icosahedra. The 30-atom structure is made up of three interpenetrating D_{3h} units. Global minima of from the 31- to 36-atom clusters also consist of several distorted icosahedra. The 37- and 38-atom structures are borrowed from Ref. [53]. The first is a distorted decahedron and the second one is a truncated octahedron. The 37-atom structure is the only structure belonging to the decahedral morphology in our calculations. The 40-atom structure may be related to the 38-atom icosahedral structure given in Ref. [86]. We have found the same 38-atom icosahedral structure at the end of the first phase of our calculations. However, the 38-atom truncated octahedron has 0.1832 eV lower in energy than the 38-atom icosahedral structure. Since this energy difference is small for $N=38$, (it is almost a degenerate state), the dip and the peak in Fig.IV.2 for this size are not well pronounced.

The 39-, and from the 41- to 49-atom clusters contain a pentagonal bipyramids in their cores. They are all related to each others and have centred icosahedral morphology. The 50-atom global minimum is the "twinned truncated octahedron" (the initial coordinates were taken from The Cambridge Cluster Database [87] mentioned in Doye and Wales' study [53]). In our initial calculations, we have found an icosahedral structure for this size. The energy difference between the lowest energy structures of icosahedral and octahedral "funnels" of the 50-atom clusters is about 0.03116 eV, which is even smaller than the corresponding quantity of those of the above mentioned 38-atom clus-

ters. Therefore, in Fig.IV.2 there is no structure for the size of $N=50$. Between the two perfect spherical symmetries at the sizes $N=13$ and $N=54$, the energy difference between different morphologies of a given size is small. Thus, in Fig.IV.2(a-b) these sizes are oscillating around the reference lines without any pronounced dips or peaks.

The *Pt* clusters described by Voter-Chen version of the EAM potential and SC potential have common global minima at 11 sizes ($N=23, 24, 29, 30, 36, 37, 38, 42, 45, 48$ and 50). However, the EAM potential energies of these structures are significantly smaller than the SC potential energies for all of these sizes. For instance, the SC potential energy of the 23-atom global minimum structure is 118.814 eV, whereas the EAM potential energy of the same structure is 107.231 eV. The energy difference between the two models increases as the size increases, and it reaches up to 19.595 eV at $N=50$. Both of Voter-Chen and SC potentials are spherically symmetric and both of them have many-body parts. The main difference between them is the fact that the Voter and Chen version of the EAM potential is derived by fitting simultaneously to the properties of the diatomic molecule and the bulk platinum, however the parameters of the SC potential are derived by fitting to those of only the bulk platinum. Therefore, we expect that the Voter and Chen's model is more suitable for the small clusters. This may also be one of the reasons to explain different results of the global minima reported in this paper and in the Ref. [53].

CHAPTER V

MELTING BEHAVIOR OF THE CLUSTERS

V.1 Computational Details

In order to investigate the temperature dependent behavior of the Pt_N clusters ($N=12-14, 54-56$), we have calculated the time average of the root-mean-square (RMS) bond-length fluctuations and that of the coordination number (CN) of individual atoms over a time interval of 5 ns at different temperatures (5 ns correspond to 5 million MD steps in the phase-space of the clusters since a single time step is of 10^{-15} s). Before starting to calculate the time average of these physical quantities, the clusters are equilibrated first (for 5 million time steps) in the MD at each total energy. Starting from very low temperatures (less than 10 K), we have increased the total energies of the clusters by 0.1 % of the total energy in a stepwise manner and recorded the time averages of the physical quantities at 161 different temperatures (up to 2500 K). The cluster

temperature, $T(K)$, is calculated by

$$T(K) = \frac{2 \langle E_k \rangle}{(3N - 6)k} \quad (\text{V.1})$$

where E_k is the total kinetic energy, the $3N - 6$ is the internal degrees of freedom of the cluster, and k is the Boltzmann constant. The time averaged atomic RMS bond-length fluctuations are calculated from the equation

$$\delta_i = \frac{1}{N - 1} \sum_{j \neq i} \frac{(\langle r_{ij}^2 \rangle - \langle r_{ij} \rangle^2)^{1/2}}{\langle r_{ij} \rangle} \quad (\text{V.2})$$

where r_{ij} is the distance between the atoms i and j , and $\langle \rangle$ denotes the time average over a single run (5 ns). Heat capacities per atom, C_v , of all the clusters have also been calculated. The C_v per atom [88] is obtained from the equation

$$C_v = k \left[N - N \left(1 - \frac{2}{3N - 6} \right) \langle E_k \rangle \langle E_k^{-1} \rangle \right]^{-1}. \quad (\text{V.3})$$

Although the equation above is formulated for canonical ensemble, it can be seen in the Ref. [89] that the difference in the canonical and microcanonical specific heats is only moderate even for 7-atom cluster, and it practically vanishes for 55-atom and, even more so, for 147-atom cluster.

V.2 Results

Previous theoretical studies show that melting temperatures of small clusters are strongly related to their sizes, structures and two-stage melting takes place for the clusters at certain sizes [90]. Lee and co-workers [91, 92] presented an atom-resolved analysis of surface melting in Ni_N clusters ($N = 12 - 14$)

modelled by the tight binding method by using the standard Monte Carlo simulation technique. We have presented RMS bond-length fluctuations, average CN s of each atoms and heat capacity curves of 12-, 13- and 14-atom Pt clusters in Fig.V.1, Fig.V.2, Fig.V.3 and those of 54-, 55- and 56-atom clusters in Fig.V.4, Fig.V.5, and Fig.V.6 respectively.

The global minimum structure of the Pt_{12} cluster, which is an icosahedron with a vacancy on the surface, has three topologically distinct sites with 5, 6 and 11 CN s, initially. As seen in the middle plot of Fig.V.1, all atoms in this structure preserve their CN s up to nearly 850 K. Similarly, RMS fluctuations in bond-length (top plot in Fig.V.1) change linearly up to this temperature. Thus, the cluster simply expands without losing its structural identity up to 850 K. Above 850 K, atoms are able to interchange their positions in the cluster, therefore their CN s start to change. As the temperature increases further, the icosahedral structure starts to deform. For instance, there is no stable central atom with $CN=11$ any more after 1000 K. The continuous positional interchanges between the atoms of the cluster and then the structural deformation result in a rapid increase in RMS bond-length fluctuations of the atoms (see the top plot in Fig.V.1). This rapid increase in RMS bond-length fluctuations of the atoms is continuous between 850 K and 1400 K for Pt_{12} cluster. During this melting stage the RMS bond-length fluctuations of the individual atoms do not overlap unlike the solid-like (0 K - 850 K) and liquid-like (above 1400 K) phases. In the heat capacity curve of the Pt_{12} cluster there is a peak at about 1650 K (this peak begins to rise rapidly above 1300 K),

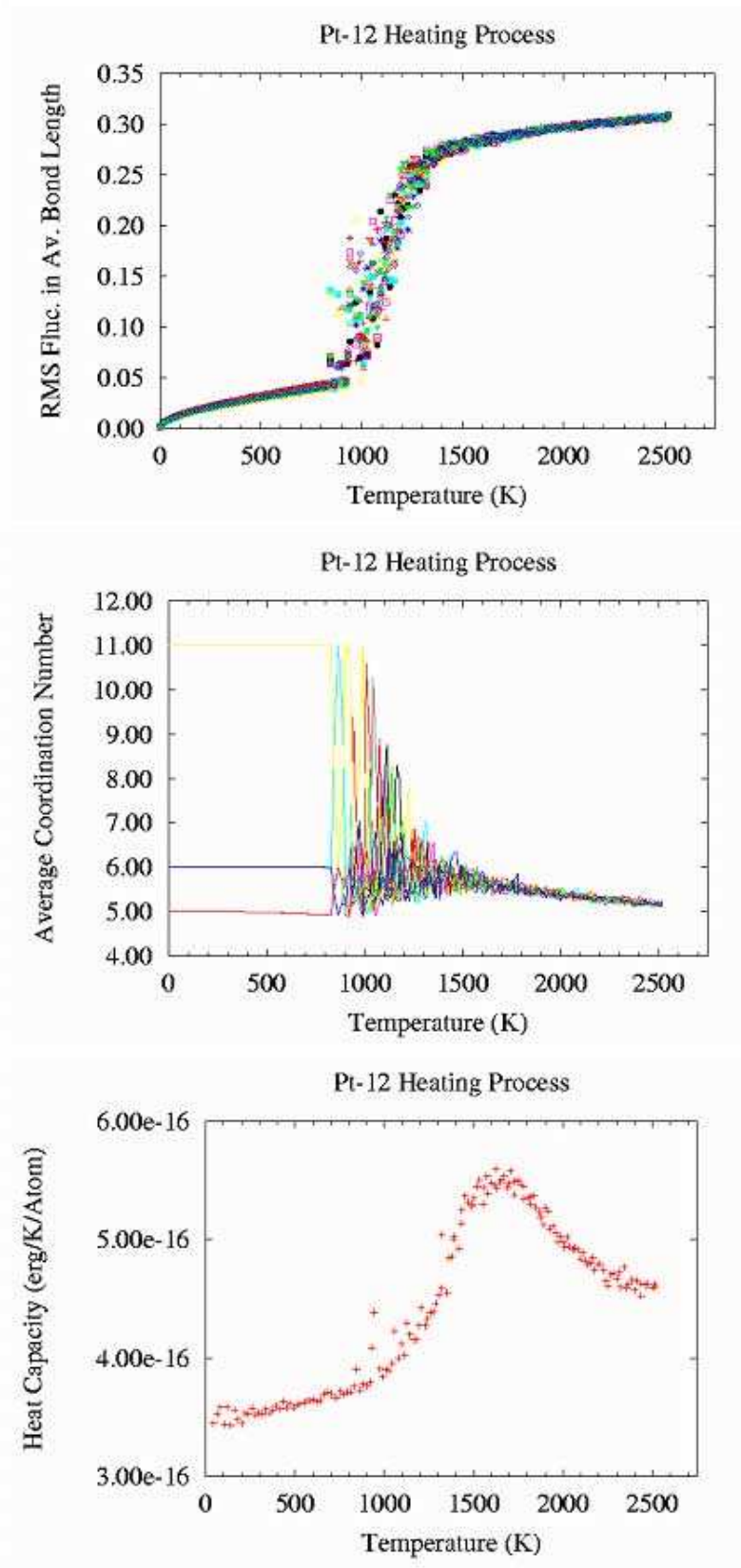


Figure V.1: Heating process of Pt_{12} cluster

which we prefer to define as "fully" liquid phase of the cluster. After 1300 K temperature (in the liquid phase) all atoms in the cluster have approximately the same CN , and gradual thermal expansion of the cluster is observed.

The melting process of the Pt_{13} icosahedron is similar to that of 12-atom cluster. The phase changes start at about 1450 K (see top and middle plots in Fig.V.2) and the cluster is in the liquid phase above 1800 K, where the peak in the heat capacity curve begins to rise rapidly (see bottom of Fig.V.2). The melting behavior of the 14-atom icosahedron with an adatom on the surface is different from the previous two clusters. In all of the plots in Fig.V.3 it can be seen that the Pt_{14} cluster undergoes two-stage melting. The adatom of the Pt_{14} cluster having CN 3 starts to hop on the surface of the icosahedron at about 300 K. Up to this temperature the CN of some of the surface atoms are 6, while that of some other surface atoms is 7. When the temperature reaches 500 K, the adatom accommodates itself among the 12 surface atoms (into the shell). Therefore, after this temperature we do not observe any atom with CN of 3. Between the temperatures of 500 K and 1200 K while all the 13 surface atoms (formerly 12 of them were surface atoms and 1 was an adatom) moves on the surface of the icosahedron, the central atom, which has a CN of 12, does not lose its central position. The first interchange between the central atom and any of the surface atoms occurs at about 1200 K. As the internal energy increases, this interchange becomes more frequent. Above 1500 K the cluster loses its shell structure (there is no atom with a $CN=12$ any more) and the cluster "melts". At higher temperatures the CN values merge gradually

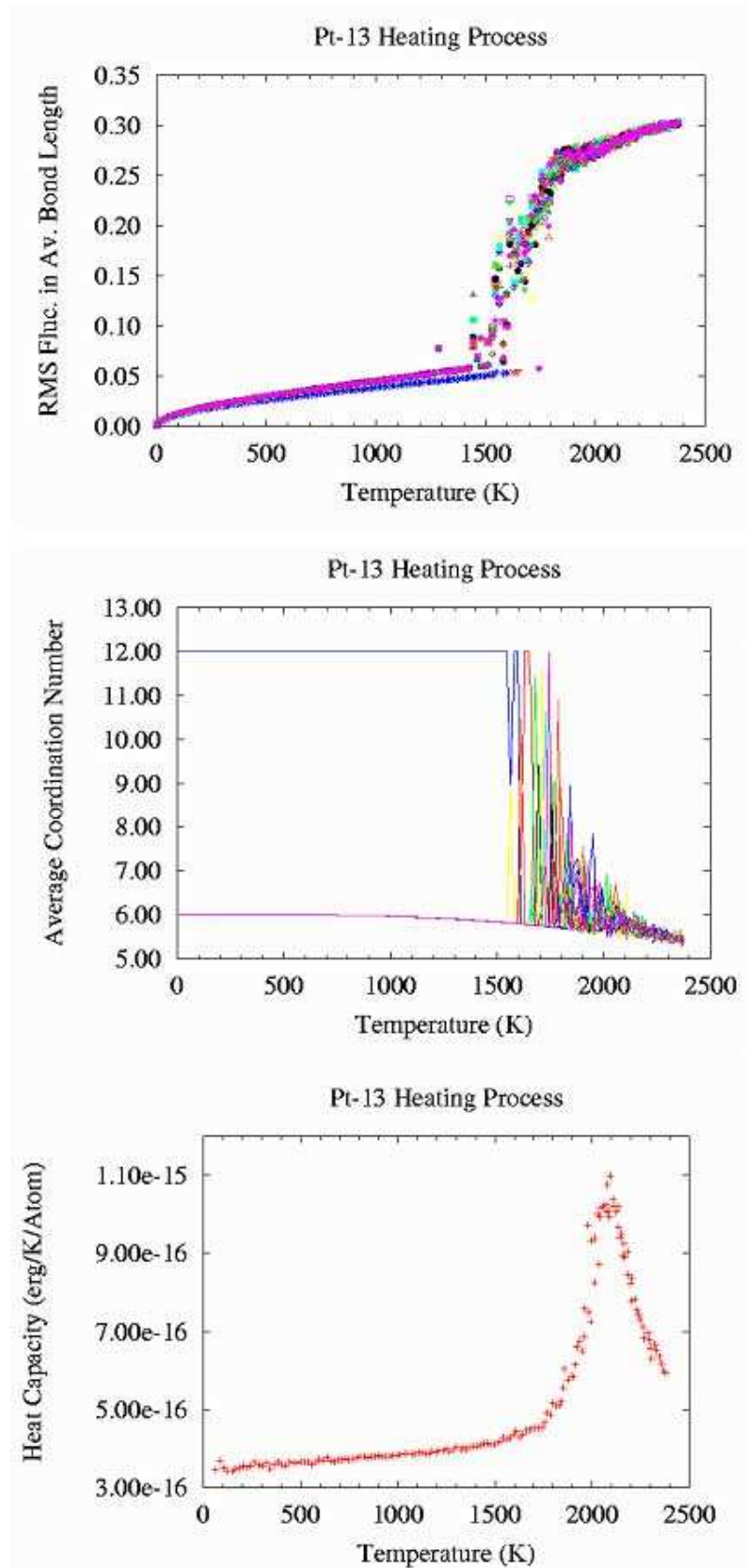


Figure V.2: Heating process of Pt_{13} cluster

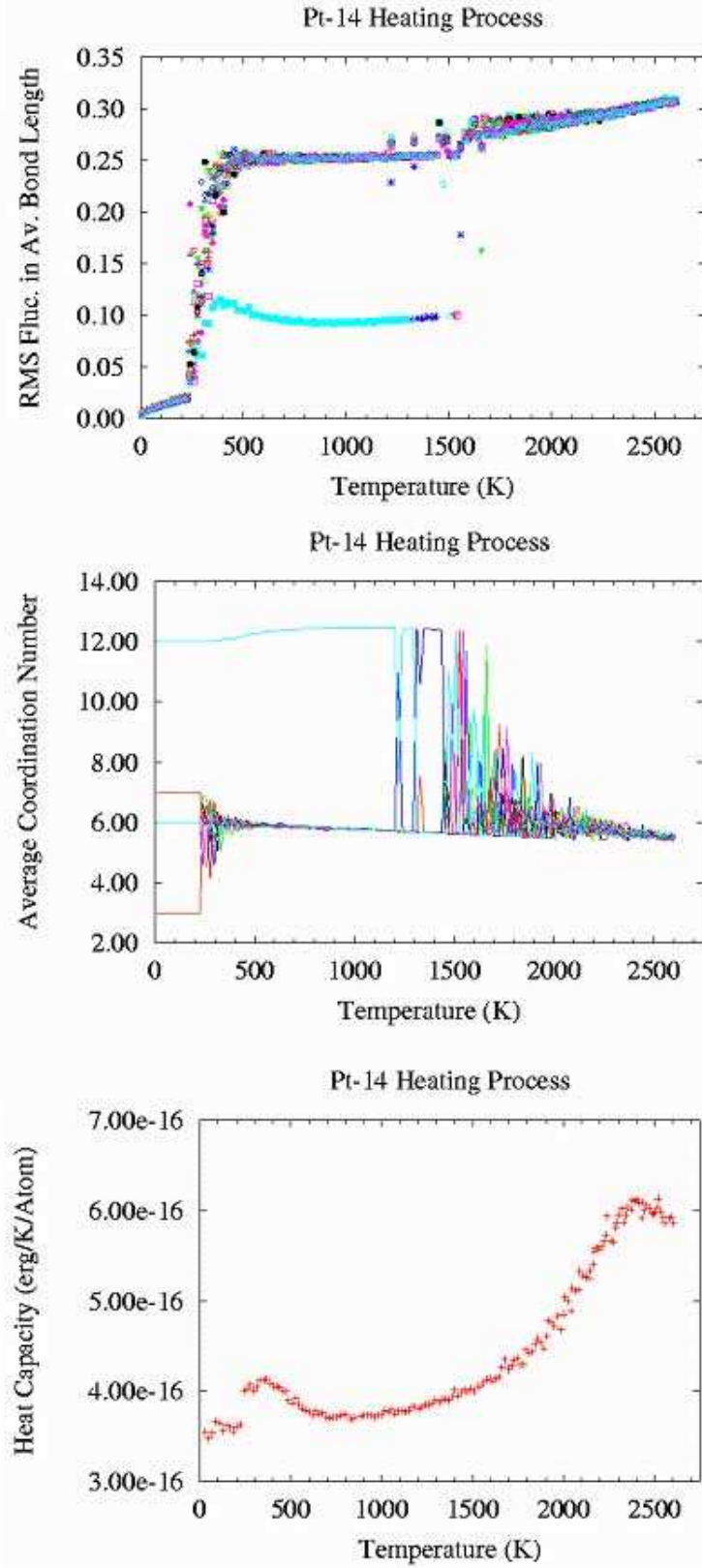


Figure V.3: Heating process of Pt_{14} cluster

to 6. In the top plot of Fig.V.3 there are two stages of rapid increase in RMS bond-length fluctuations of individual atoms. Similarly, there are two peaks in the heat capacity curve. The slope of the first peak increases above 250 K which coincides with the premelting, and the second peak rises rapidly above 1500 K which represents the actual melting of the cluster. Gradual thermal expansion of the cluster continues after this temperature, and the specific heat has a second peak at 2400 K.

The global minimum structure of the Pt_{54} cluster, which is the uncentred icosahedron (see Fig.IV.4), consist of two spherical shells. The number of the nearest neighbors (CN) of all inner shell atoms is 11, whereas some of the atoms on the outer shell have 6, some of them have 8 nearest neighbors. As seen in the middle plot of Fig.V.4, all atoms in this structure preserve their CNs up to nearly 950 K. Similarly, RMS fluctuations in bond-length (top plot in Fig.V.4) change linearly up to this temperature. Thus, the cluster is in the solid phase and simply expands without losing its structural identity up to 950 K. Above 950 K, atoms are able to interchange their positions in the cluster, therefore their CNs start to change. Between 950 K and 1050 K, CNs of some atoms are greater than 11 which indicates that the common center of the inner and the outer shells is occupied by one of these atoms. As the temperature increases further, the icosahedral structure starts to deform. For instance after 1050 K, there is neither an atom with $CN=11$ nor $CN=6$. The continuous positional interchanges between the atoms of the cluster and then the structural deformation result in a rapid increase in RMS bond-length

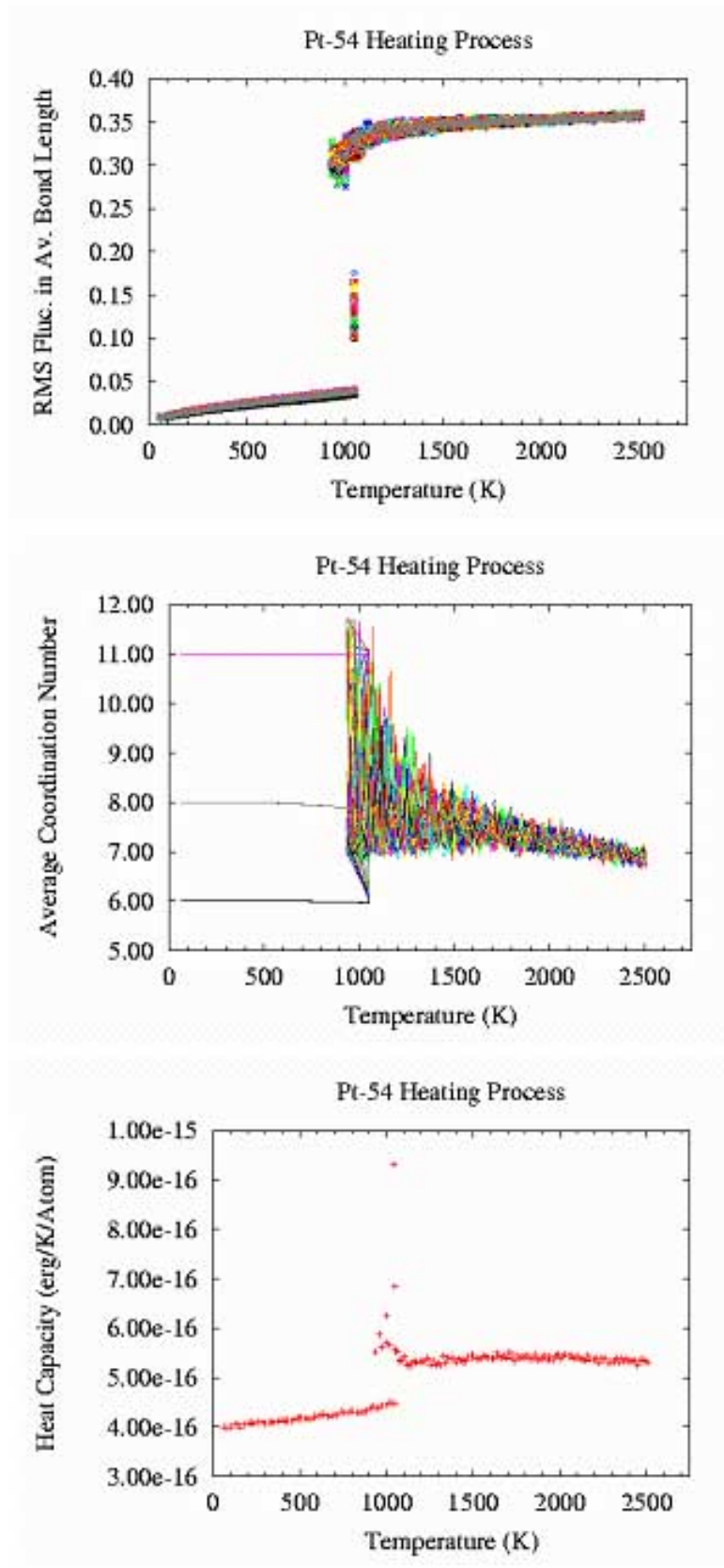


Figure V.4: Heating process of Pt_{54} cluster

fluctuations of the atoms (see the top plot in Fig.V.4). This rapid increase in RMS bond-length fluctuations occurs at different but near temperatures between 950 K and 1100 K for each atom of the Pt_{54} cluster. Accordingly, the heat capacity curve of the Pt_{54} cluster fluctuates between these temperatures and reaches a peak value at about 1050 K. The heat capacity curve starts to change linearly after 1100 K again, which we prefer to define as "fully" liquid phase of the cluster. Thus, the fluctuation in the heat capacity curve of the cluster between 950 K and 1100 K is due to the fact that the maximum contribution of each atom in a cluster to the heat capacity curve occurs at different temperatures unlike the atoms of the bulk. After 1100 K temperature, the cluster is in the liquid phase and expands gradually. At about 1500 K, all CN s are between 7 and 8. As the temperature increases further, the CN values of all of the atoms in the cluster are merging towards 7.

The global minimum structure of the 55-atom Pt cluster is the centered icosahedron. The single atom in the center of the icosahedron produces the differences in the melting behavior between the Pt_{55} and the Pt_{54} clusters, which can be seen in Fig.V.5. First of all, the melting process starts at about 800 K for the Pt_{55} cluster (see the middle plot in Fig.V.5), which is less than 950 K of Pt_{54} cluster. Secondly, the contributions of the surface and core atoms of the Pt_{55} cluster to the melting process are more separable than those of the Pt_{54} cluster (see the top plots in Fig.V.4 and Fig.V.5) since the central atom of the Pt_{55} cluster makes the remaining 12 core atoms stronger. The two groups of atoms seen in the top plot of Fig.V.5 (the RMS bond-length

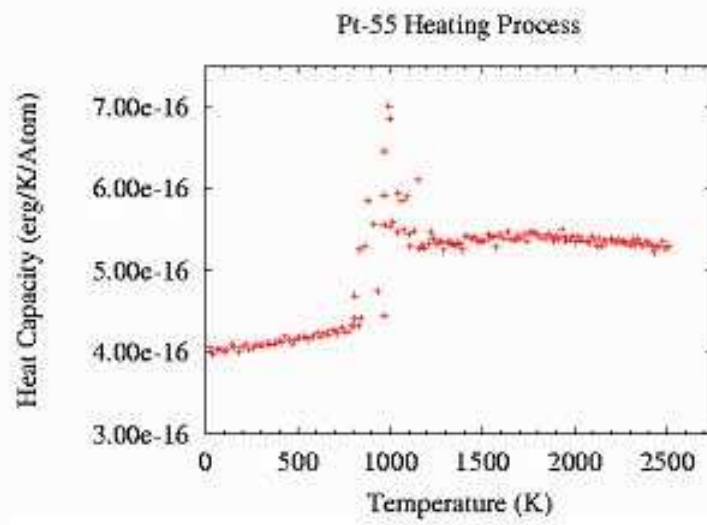
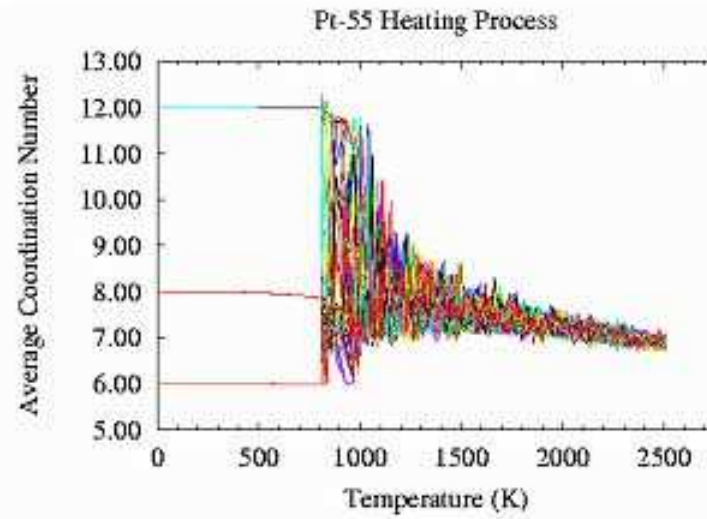
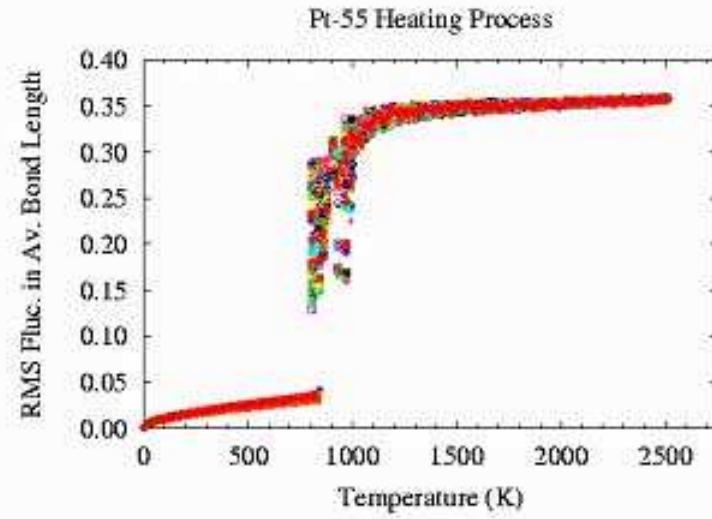


Figure V.5: Heating process of Pt_{55} cluster

fluctuations of the first group increase rapidly at about 850 K, where as those of the second group increase rapidly at about 950 K) correspond to the surface and the core atoms of the structure. In the heat capacity curve of the Pt_{55} cluster, the nonlinear part is wider (between 800 K and 1150 K). After 1150 K, the Pt_{55} cluster is in "fully" liquid face. Therefore, the surface melting of the centred 55-atom icosahedron starts earlier than the uncentred 54-atom icosahedron, but the centred 55-atom icosahedron melts totally at a slightly higher temperature than the uncentred 54-atom icosahedron.

The lowest energy structure of the 56-atom Pt cluster belongs to the uncentred icosahedral morphology (see Fig.IV.4). The main difference of the melting behavior of the Pt_{56} cluster from those of the previous two clusters can be seen in the middle plot of Fig.V.6. In the mentioned plot it can easily be noticed that the surface atoms of the Pt_{56} cluster start to interchange their positions at about 400 K as well as the core atoms. In between 400 K and 700K, a surface atom can change its position with another surface atom or a core atom can change its position with another core atom but, a positional interchange between a core and a surface atom never occurs. The first such interchange is observed above 700 K and it continuous up to 1100 K. Above 1100 K, the icosahedral symmetry is already lost. The top and the bottom plots of Fig.V.6 can be interpreted accordingly. The RMS bond-length fluctuations of all atoms in the Pt_{56} cluster increase slightly together up to 400 K. The positional interchanges among the surface and among the core atoms result in different RMS bond-length fluctuations between 400 K and 700 K.

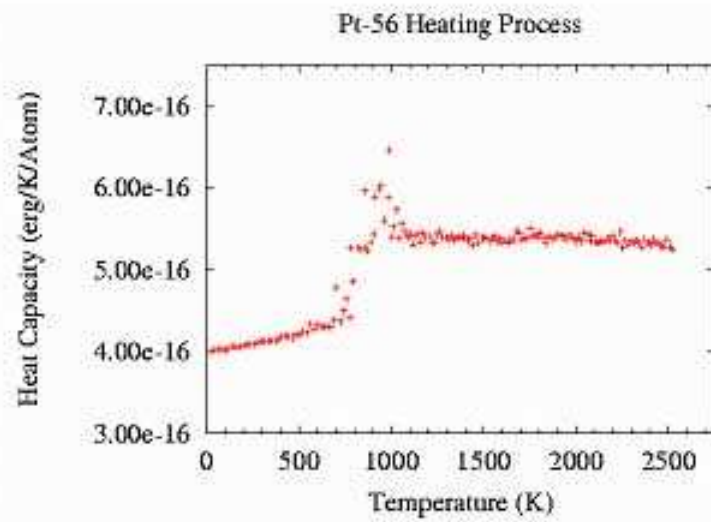
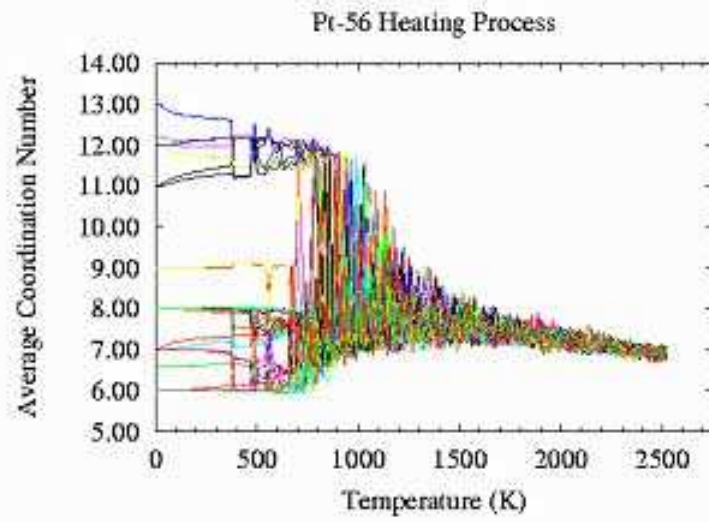
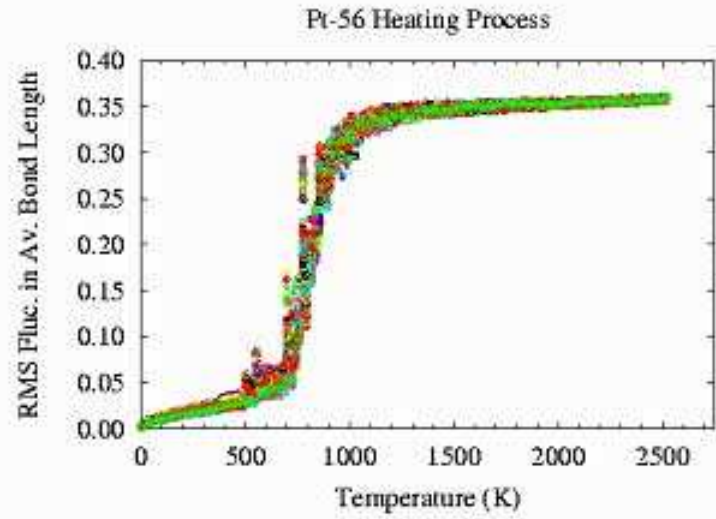


Figure V.6: Heating process of Pt_{56} cluster

When the atoms can move in the cluster longer distances, rapid increase in the RMS bond-length fluctuations is observed (between 700 K and 1100 K). The nonlinear part of the heat capacity curve of the Pt_{56} cluster between these temperatures is due to the above mentioned motions of the atoms. After 1100 K, the heat capacity curve of the 56-atom Pt cluster is again linear, which indicates that the cluster is totally in the liquid phase. In all of the mentioned six sizes, the liquid state has higher specific heat values than those of the solid form.

CHAPTER VI

Pt_{75} CLUSTER

VI.1 Computational Details

It is an extremely difficult task to find out the global minimum energy structure of a large cluster such as the one having 75 atoms, since the number of minima increases with the size exponentially. Some recent calculations on higher sizes metallic clusters can be found, for instance, in the references [93, 94]. We have searched the global minimum energy structure for this size as follow: First, a non-rotating and non-translating Pt_{75} cluster is prepared and then heated over 2600 K which is close to the fragmentation energy (at this internal energy, atoms are highly mobile). Therefore, a simulation run over 6 million steps with a step-size of 2 fs is found to be sufficient to search a phase space point which has the largest kinetic energy. After obtaining this phase space point possessing the largest kinetic energy at the mentioned constant total energy, it is quenched using several TQ runs such that during the first 10,000

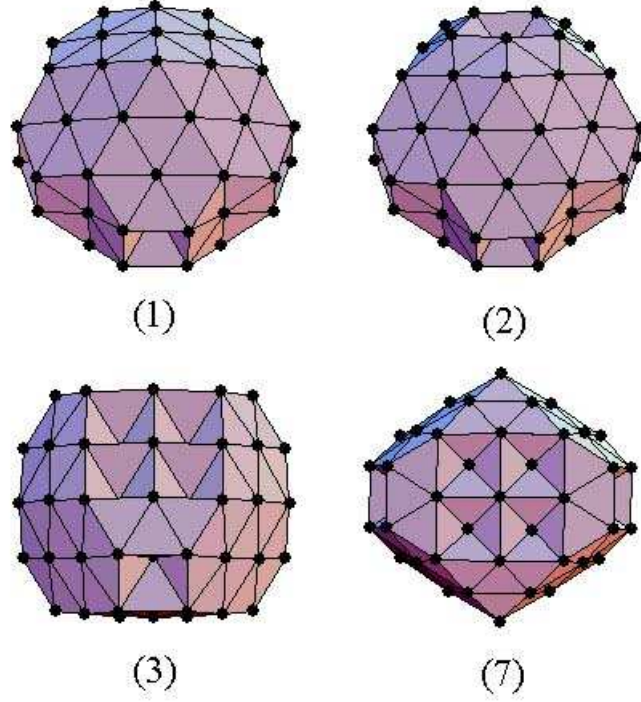


Figure VI.1: The 1st, 2nd, 3rd, and 7th locally stable structures of the Pt_{75} cluster

TQ steps internal kinetic energy is removed frequently, whereas in the later stages energy is set to zero less frequently until the entire kinetic energy is removed. The first stage of the minimization keeps the cluster in the vicinity of the selected phase space point. At the end we have obtained the global minimum energy structure of the Pt_{75} cluster which is a Marks decahedron [95] (see the left picture of the top panel in Fig.VI.1). The same structure has been reported by Doye and Wales [53] as the lowest energy structure of 75-atom platinum and gold clusters in their study where they have employed the Sutton-Chen potential and obtained the energy of the global minimum structure as -405.23 eV. However, our corresponding energy is -379.74 eV. The difference in the energies is due to the fact that the parameters of the Sutton-Chen potential have been obtained by fitting to only the properties of

bulk platinum. They have reported that Marks decahedron is a highly stable symmetric form compared to the other sizes of the Pt_N clusters ($N < 80$) using the first and second energy differences of the clusters. The Marks decahedron is also reported by Baletto et al. [96] as the global minimum energy structure of 75-atom silver clusters in their MD simulations.

VI.2 Isomers and Isomer Spectrum

In order to investigate the correlations between the total energy of the cluster and the isomer number and between that and the ESW of the isomers, we have made 80 different MD runs at 80 different total energies (from the lowest energy up to the fragmentation energy). The total energy is increased by approximately 0.3% in each run, and the last phase space values of one run have been used as an input for the next run. Furthermore, after each 50 MD steps in a trajectory, the phase space points have been quenched by the L-BFGS conjugate-gradient routine to find the stable isomeric forms of the Pt_{75} cluster. The total length of each run is nearly 3.6 million steps which is equivalent to approximately 7 ns. Therefore, in each run 70,990 minimization attempts have been performed, however in some of these attempts the minimization could not be achieved because of the numerical errors in the derivatives. From the all of the runs (80 x 7 ns) we have obtained 1,007,811 different isomers. In Table VI.1, the quenched energies of the first 14 isomers are listed. In Fig.VI.1, we present the triangulated polyhedral structures of some of these isomers. The number in the parentheses denotes the isomer number, i.e., (1) is the global

Table VI.1: Energies of the first 14 isomers of the Pt_{75} cluster at T=0 K

Isomer Number	Energy (eV)
1	-379.741
2	-379.154
3	-379.122
4	-379.120
5	-379.080
6	-378.982
7	-378.965
8	-378.960
9	-378.958
10	-378.946
11	-378.946
12	-378.936
13	-378.933
14	-378.858

minimum energy structure, and so on.

It can be seen in Table VI.1 that the energy differences between the successive isomers are very small, except the spacing between the first and the second isomers, (the global minimum energy structure is somewhat separated from the others). The isomers presented in Fig.VI.1 have different structural morphologies. The $Pt_{75}(1)$ and the $Pt_{75}(2)$ structures have decahedral symmetries, whereas the $Pt_{75}(3)$ is a face-centered cubic (fcc) closed-packed structure and the $Pt_{75}(7)$ belongs to the icosahedral morphology. All of the three main types of the ordered packing, i.e., decahedral, face-centered cubic and icosahedral, seen in the smaller clusters found in this study too. Although there are small energy differences between the minima of these structures (different structural morphologies), high potential energy barriers separate them.

In Fig.VI.2 we present temperature dependencies of the isomer number (N_i) and the corresponding ESW. As seen in the figure, the isomers' ESW is zero

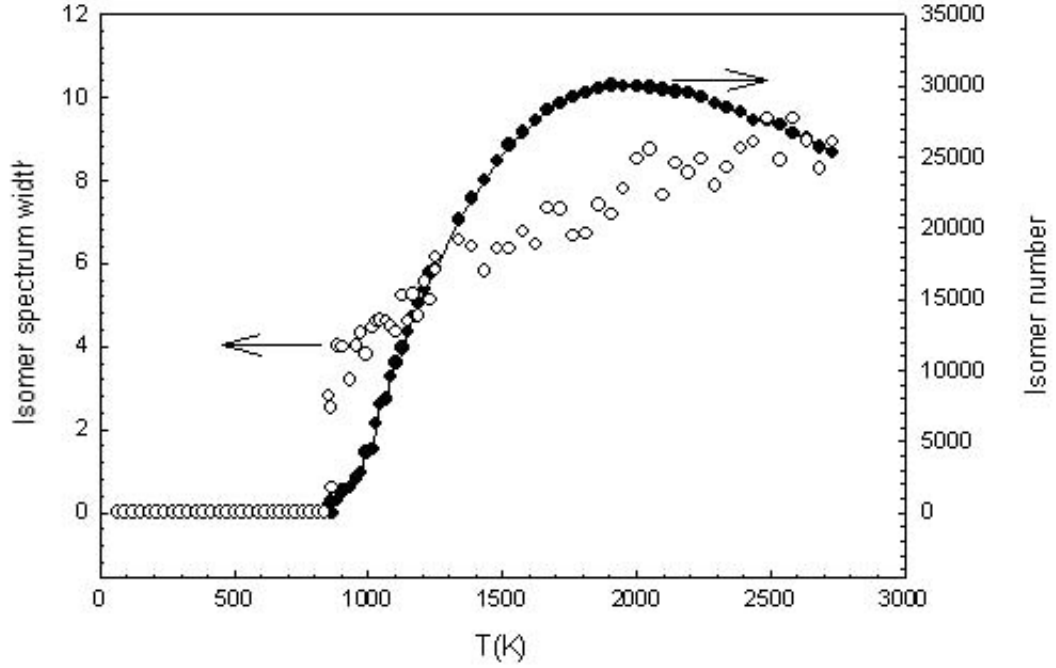


Figure VI.2: Correlations between isomer-energy-spectrum and isomer number with temperature

up to 850 K since no other isomers were obtained in the simulations up to this temperature. This means that potential well of the global minimum is quite deep, i.e., Marks decahedron is highly stable, and preserves its symmetric solid-like form. Above 850 K the second and higher energy isomers are "visited", therefore the ESW is increasing rapidly as temperature increases. After 1000 K, the ESW is a monotonically increasing function of temperature up to the fragmentation temperature (2750 K). As expected, the N_i is equal to 1 up to 850 K, and increasing rapidly above this temperature. The N_i is reaching to a threshold value of approximately 30,000 isomers which are obtained in a single trajectory near 1900 K. The rate of increase in the N_i is higher than the rate of increase in the ESW since most of the isomers are closely spaced in energy. Since the cluster is fully melted at about 1900 K and the most of

the isomers are accessible around this internal energy, within the 7 ns run, similar numbers of N_i are "visited" around this temperature. The decrease of N_i above 1900 K can be explained as the following: When the cluster is fully melted, it starts to spend more time (in a given observation time) "over" some number of high-lying local minima which are too shallow. Those shallow wells are causing errors in numerical derivatives. Therefore some of the observation time is lost, and as a result, less number of isomers is obtained. Secondly, the starting phase space of each trajectory affects N_i . Since the end phase space values of one run are used as an input for the next run the cluster may not "visit" many basins of attractions which have been "visited" in the previous run. However, in any case a threshold value would be reached for a limited observation time.

The isomer number (N_i) as a function of the isomer energy (E) discussed in detail for the first time in this paper (see Fig.VI.3) up to our knowledge. From this curve, one can extract the rate of change of N_i with E as dN_i/dE . As seen from Fig.VI.3, the N_i has two asymptotic values or dE/dN_i has two singularities. These two asymptotic regions correspond to two different physical states. One of the asymptotic values is approaching to the value of 1 which corresponds to the global minimum energy structure, and the second one towards the highest energy isomer (close to the fragmentation stage) is approaching to the total number of isomers, 1,007,811. The rate of change towards the asymptotic regions, i.e., above -373 eV and below -378 eV energies, is so small that there are a few isomers per unit energy interval. On the other

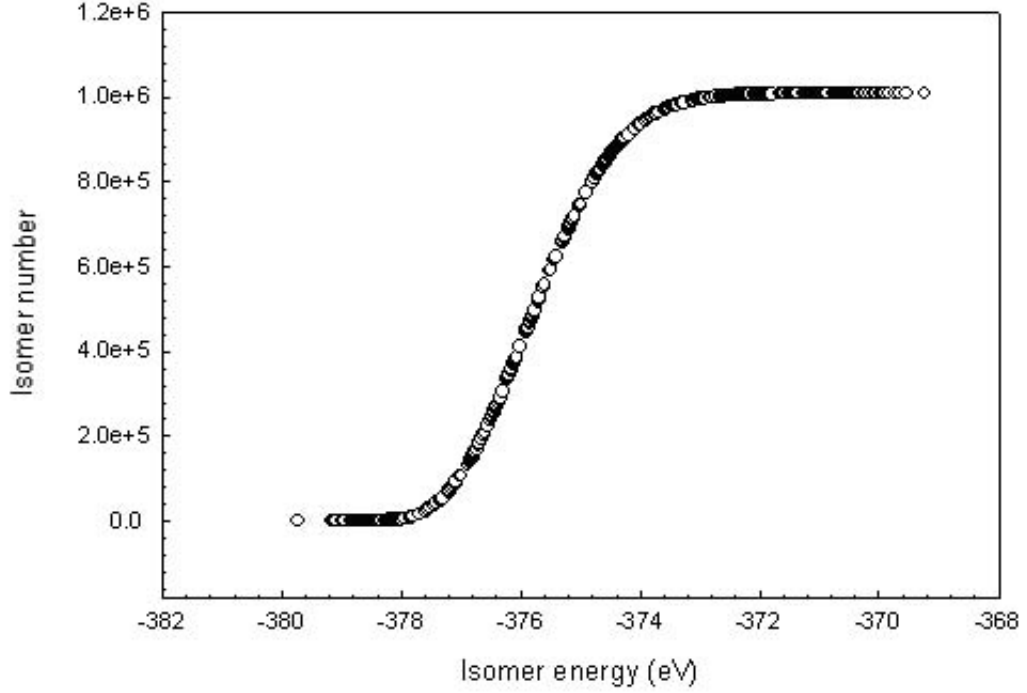


Figure VI.3: Isomer number versus isomer energy in units of eV

hand, the energies in between -378 eV and -373 eV, the rate (slope) is high and nearly constant, (has stretched S-like shape). Within 5 eV energy range we have obtained over 1,000,000 isomers (see Fig.VI.3). The total ESW of all of 1,007,811 isomers is 10.76 eV. Thus, the majority of the isomers are concentrated within a half of the total ESW, and towards the asymptotic regions isomers are energetically more separated.

The isomer finding probability, $P_i(T)$, is defined as $P_i(T) = N_i(T)/N_{tot}$, where $N_i(T)$ denotes the number of times i^{th} isomer visited and N_{tot} denotes the total number of attempts ($N_{tot}=70,990$). The probability distribution as a function of temperature is investigated. Since the cluster is in the global minimum energy structure up to 850 K, the probability is one for the 1st isomer in the temperature interval from 0 K to 850 K. Near 854 K, $P_1 = 0.998$

and $P_2=0.014$. Just above 854K, $P_1=0.393$, whereas $P_2=0.037$, and $P_3=0.062$. However, above 900 K, P_1 becomes rapidly smaller since tens of thousands of isomers are accessible at those energies, and our observation time is constant (7 ns). Near 1500 K and up, P_1 becomes even zero (never has a chance to visit again the global minimum). Therefore, one can easily conclude that the probability of finding a specific isomer highly depends on the initial conditions of the trajectory. The starting configuration and the total energy of the cluster as well as the observation time are the factors that determine the probability. Nevertheless, since the global minimum structure of the Pt_{75} cluster (Marks decahedron) remains in its symmetric form up to 850 K, it may be detected using the chemical probe experimental technique [83] .

VI.3 Phase Changes and Melting

The phase change dynamics of the Pt_{75} cluster are monitored by observing the changes in the short-time averaged kinetic energies (temperature) of the cluster. In order to test the level of "stability" of the 1st isomer, we have heated the cluster in a stepwise manner starting from T=0 K. In Fig.VI.4 short-time averaged temperatures, $\langle T(K) \rangle$ s, related to this observation are plotted as a function of time intervals; for each time intervals one short-time average is calculated, and one time interval is 250 time steps.

The average is taken to reduce the fluctuations in the kinetic energy due to the vibrational motions of the atoms about their equilibrium positions. Since these oscillations are hindered, changes in the averaged kinetic energies due

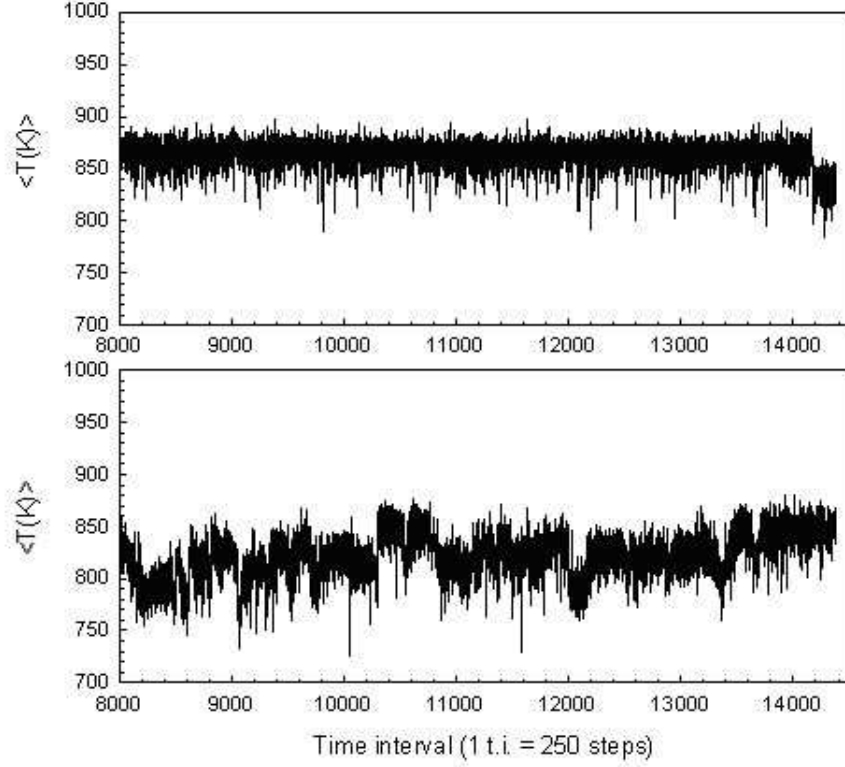


Figure VI.4: Short-time averaged temperatures as a function of time interval

to the phase changes become visible. As seen from Fig.VI.4, the first phase change from the 1st isomer to the 2nd one takes place at -362.72 eV of total energy which corresponds to approximately 865 K. Thus, the upper limit of the potential energy barrier between the 1st and the 2nd isomers is about 379.74-362.72=17.02 eV. In the run which has slightly higher total energy (-362.15 eV), within the 7 ns observation time, cluster visits frequently many other potential wells (not shown). Above 900 K, there are many other potential wells which are accessible. Therefore, after moving out of the 1st isomer's potential well the cluster hardly visits again the lowest energy phase.

The RMS values of 75 atoms are shown for each temperature in Fig.VI.5. As seen, no pre-melting is observed in the temperature interval of 0 - 850 K.

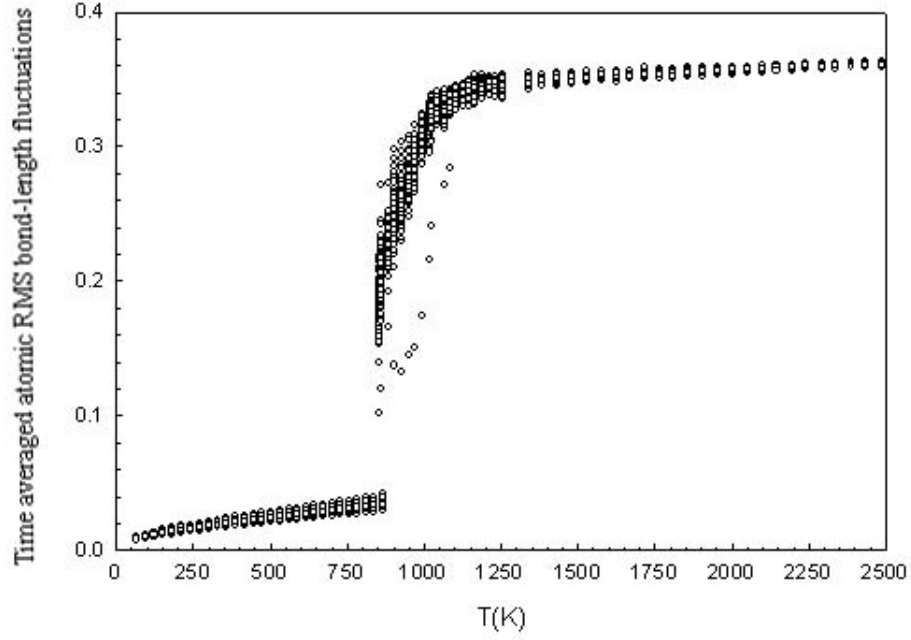


Figure VI.5: Time averaged atomic RMS bond-length fluctuations as a function of temperature

The pre-melting phenomenon is discussed in detail in the previous chapter. All atoms remain in tack with small oscillations around the equilibrium positions up to 850 K. Only normal thermal expansion of the cluster has been observed. The sudden jumps in the fluctuations of all the atoms near 865 K indicate that all atoms move collectively to change the structure from the 1st isomeric form to the 2nd one. Three atoms near 865 K have relatively less RMS fluctuations than the others as seen in Fig.VI.5. At the next total energy, this number is reduced to two. After that there is only one atom which has quite lower RMS value compared to the others. This atom remains different in fluctuations than the others from 900 K to 1150 K. Above 1150 K differences in fluctuations are getting smaller with increasing temperature. The physical locations of the atoms affect their fluctuations. Above 900 K atoms in the cluster have better chance to move from a stiff form to a more relaxed structure. Thus, only one

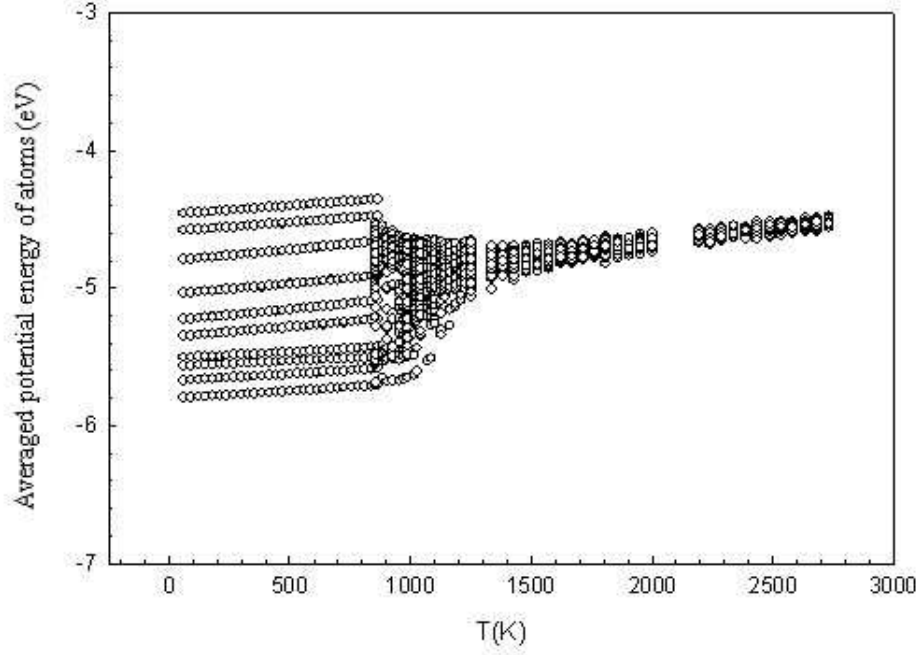


Figure VI.6: Time averaged potential energies of all of the atoms as a function of temperature

of the atoms is more localized inside the cluster between 900 K and 1150 K, therefore it has a substantially lower value among the fluctuations. At higher temperatures differences between the RMS fluctuations of the atoms are much smaller, which indicate that the cluster is fully in liquid-like state. The time averaged fluctuations merge into nearly the same value after 1500 K. The cluster's melting temperature is estimated to be about 900 K, if we assume that melting begins at the mid-point of the RMS values.

In Fig.VI.6, time averaged atomic potential energies of all the atoms are presented as a function of $T(K)$. It can be seen in this figure that there are 10 different topological sites in the cluster up to 850 K. Due to the thermal expansion, averaged potential energies are increasing, and there are no exchanges between the atoms at those locations in between 0 K and 850 K. The highest

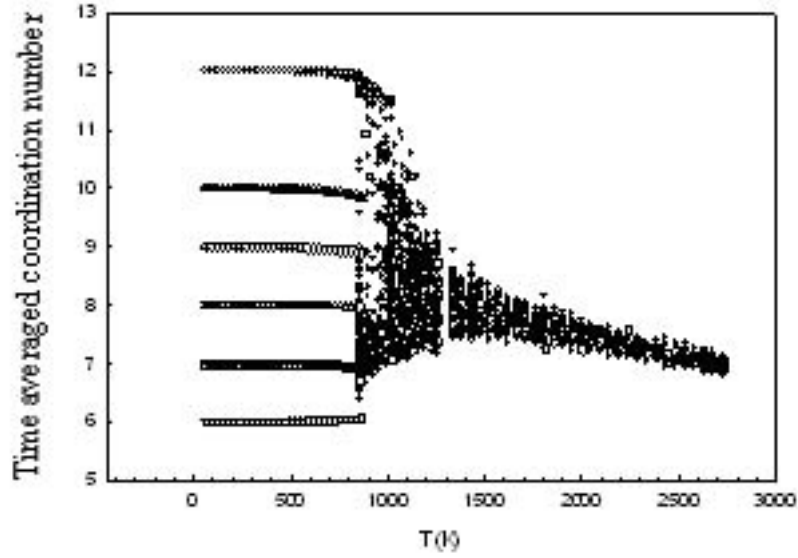


Figure VI.7: Time averaged coordination numbers as a function of temperature

potential energy particles are the surface atoms (top several rows), and the lowest several energy rows belong to the inner atoms. At and above 865 K atoms are exchanging their locations (structured potential energy lines are not seen), as inner atoms are moving outward, the surface atoms are moving inwards. As the temperature increases further, time averaged potential energies of all the atoms merge towards a single value in the fully liquid-like state.

The CN s of all atoms are averaged over the each entire 7 ns runs, and they are presented in Fig.VI.7. This figure also shows well-defined six different binding sites of the atoms up to 850 K. The atoms with $CN < 10$ are considered as the surface atoms, whereas the others are called as inner atoms. The six open symbols other than filled circles are used in Fig.VI.7 to show how and where those atoms move between the sites (one type of open symbols is used for one binding site). As seen, at and above melting temperature inner and surface atoms are exchanging their places. With increasing temperature

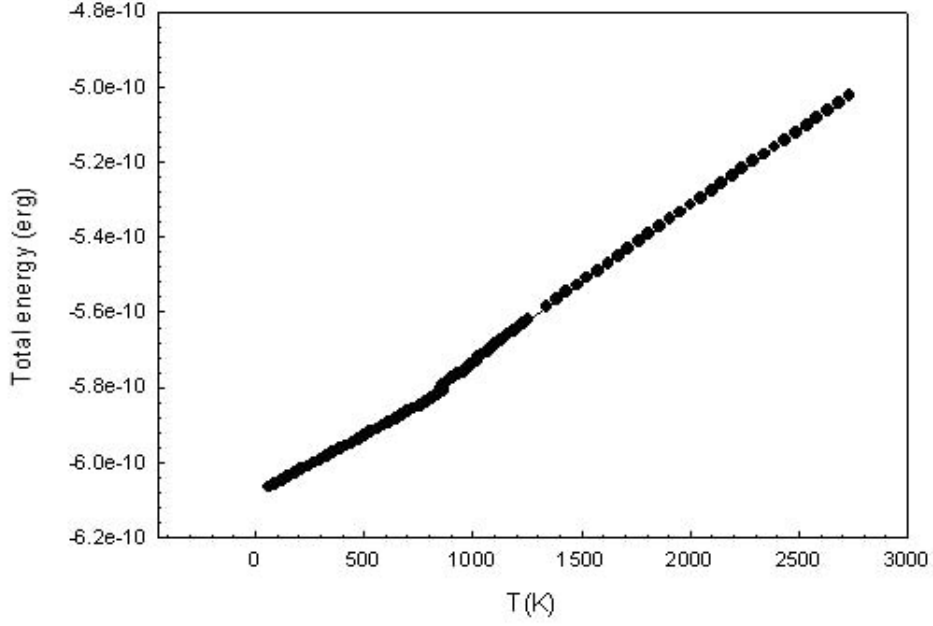


Figure VI.8: Caloric curve of the Pt_{75}

these exchanges become more rapid and differences between the CN s become smaller. Near fragmentation temperature all CN s are merging to a value of 7. The melting of the Pt_{75} cluster is also displayed by the caloric curve in Fig.VI.8.

The change in the slope of the curve at about 865 K indicates the beginning of the phase change from the solid-like to the liquid-like forms. This temperature is in good agreement with the predictions of the time averaged atomic RMSs, atomic potentials, and the CN calculations. Another tool to study the phase changes is the calculation of the specific heat (C_v) of the cluster as a function of temperature (see Fig.VI.9).

The specific-heat values for the solid form are increasing gradually with the temperature. The peak near 900 K also shows the phase transition. After the transition, the specific-heat values are decreasing gradually. However, as seen,

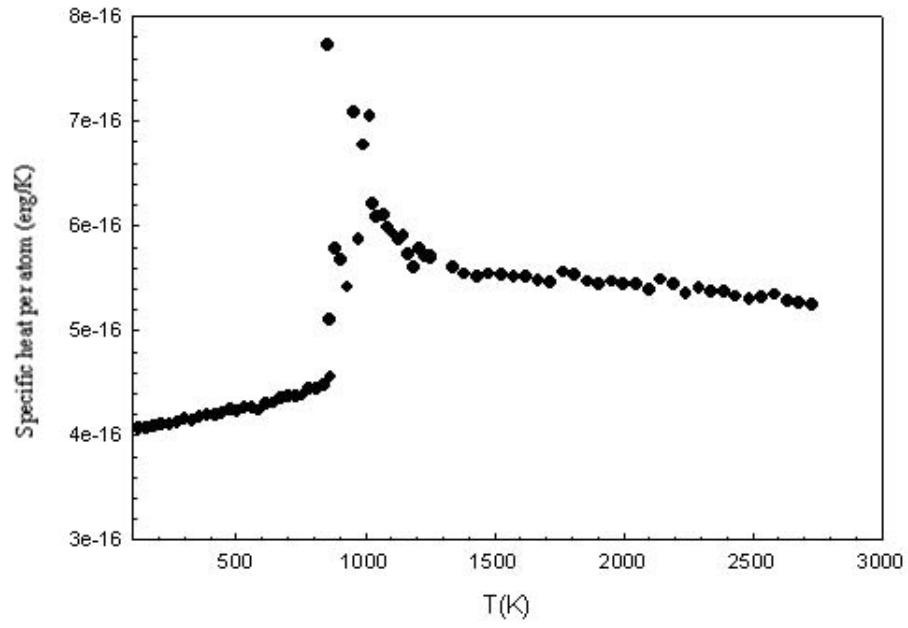


Figure VI.9: Specific heat versus temperature of the Pt_{75}

the liquid state has higher specific heat values than those of the solid form.

CHAPTER VII

CONCLUSIONS

In this study, using the constant-energy molecular dynamics simulation, thermal and conjugate-gradient minimization techniques, the global minima and the other locally stable structures, energetics, growth patterns, finding probabilities and the melting behavior of free platinum clusters in the size range of $N=2-56$ and $N=75$ are investigated by employing the Voter and Chen version of an embedded-atom model.

The results for $Pt_2 - Pt_{21}$ clusters show that many of the lowest energy structures correspond to the icosahedral growth, which are also global minima for Lennard-Jones or Morse potentials. However, some of the global minima (e.g. $N=15,16,17,18,20$, and 21) do not obey the icosahedral growth pattern. All locally stable structures of the Pt_N clusters ($N=5-21$) have either one or more of the trigonal, tetragonal, pentagonal, or hexagonal bipyramids as their backbones. It is found that, in general, isomers sampling probability distributions fall exponentially as the total energies of the isomers increase. However,

the energy dependence of the probabilities is not simple. The simple growth path, the number of accessibility from the structure of the previous size, the backbone and the symmetry of the cluster also affect the sampling probability of a specific isomer. The lowest energy structures are not the most probable isomers for some of the sizes (e.g., $N=7,14,16-19$, and 20) at very low temperatures. The total energy of the initial configurations affects the probability of sampling the basins of attractions. However, the trend (exponential decay) of the sampling probability distribution remains unchanged. The stability of the structures as a function of temperature and the influence of temperature on the growth paths can be discussed in detail in the future works.

For the size range of $N=22-56$, we have found out that all the global minima have one of the octahedral, decahedral, centred or uncentred icosahedral morphologies. Although the 38-atom global minimum structure is a truncated octahedron, 50-atom structure is a "twined truncated octahedron" and 37-atom structure is a distorted decahedron, the smaller sizes of all the other global minima have centred icosahedral and the larger ones have uncentred icosahedral morphologies. The 54-atom uncentred icosahedron is found to be more stable than 55-atom centred icosahedron.

When the melting behavior of the clusters is concerned, as the temperature increases, the 12- and 13-atom Pt clusters exhibit one-stage melting, while the 14-atom cluster with an adatom on the icosahedral surface undergoes two-stage melting. When these clusters are totally melted all of the atoms in the clusters have approximately the same $CN=6$. The melting processes are generally

started by the positional interchanges among the atoms having similar CN s. The surface melting of the centred 55-atom icosahedron starts earlier than the uncentred 54-atom icosahedron, but the centred 55-atom icosahedron fully melts at slightly higher temperature than the uncentred 54-atom icosahedron. The melting process of the 56-atom Pt cluster starts earliest, however its total melting occurs latest (transition state is much wider). When these clusters are in liquid-like state, all of the atoms in the clusters have approximately the same CN which is in this case equal to 7. In all cases, the melting phenomenon takes place over a finite temperature range (the phase transition does not take place at a given specific temperature) and the liquid state has higher specific heat values than those of the solid form.

The global minimum energy structure of the Pt_{75} cluster has the symmetry of the Marks decahedron and it is stable up to nearly 850 K. The energy difference between the highest and the lowest energetic isomers of the Pt_{75} cluster is more than 10 eV. Although it is difficult to determine the exact total number of isomers, it is shown in this study that a very big portion of the isomers are concentrated within a half of the total ESW. Towards the lowest and the highest energetic structures, isomers are energetically more separated.

Many of the results represented in our present study are in good agreement with those of other researchers. However, there are also some disagreements in the locally stable structures or in the energies of the clusters. The differences appear due to two reasons: First, the potentials used depend on different type of methods employed to describe atomic interactions, e.g. the EAM is

like effective medium type, whereas Sutton-Chen potential depends on tight-binding theory. Second, the computational procedures are different. Different minimization techniques with different initial constraints may produce different results. The low energy minima found in this study can represent good starting points for sophisticated, electronic structure (i.e. density functional theory) calculations. Since all empirical potentials have some uncertainties, it is necessary to compare the results obtained with different potentials. Therefore extensive study is necessary and important to have a good comparison of the potentials. As a result our present work creates such opportunity for the *Pt* clusters described by Voter and Chen version of the EAM in the size range of $N=2-56$ and $N=75$. In addition, the present study shows that investigating the numbers, and the structures of the stable isomers can provide a deeper understanding of the clusters' growth paths, the energy spectrum widths, energy bands and gaps formed by the isomers. It also shows that an atom-resolved analysis method including physical quantities such as the root-mean-square bond-length fluctuation and coordination number for individual atoms as functions of temperature may provide a better understanding of the melting behavior of the clusters.

REFERENCES

- [1] J. Jellinek and Z.B. Güvenç, Z. Phys. D 26, 110 (1993); J. Jellinek and Z.B. Güvenç, in *The Synergy Between Dynamics and Reactivity at Clusters and Surfaces*, L.J. Farrugia, Ed. Kluwer, Dordrecht, 1995, p.217.
- [2] H. Haberland (Ed.), *Clusters of atoms and molecules*, Springer, Berlin, 1994; and references therein.
- [3] G. Schmid (Ed.), *Clusters and colloids*, VCH, Weinheim, 1994; and references therein.
- [4] T.P. Martin (Ed.), *Large clusters of atoms and molecules*, Kluwer, Dordrecht, 1996; and references therein.
- [5] J. Jellinek (Ed.), *Theory of atomic and molecular clusters*, Springer, Berlin, 1999; and references therein.
- [6] Roy L. Johnston, *Atomic and molecular clusters*, Taylor and Francis, London, 2002; and references therein.
- [7] J.P.K. Doye, Ph.D. Thesis, Department of Chemistry, University of Cambridge (1996).
- [8] N.T. Wilson, Ph.D. Thesis, School of Chemistry, University of Birmingham (2000).
- [9] J. Westergren, Ph.D. Thesis, Department of Experimental Physics, Chalmers University of Technology and Göteborg University (2001).
- [10] D.E. Powers, S.G. Hansen, M.E. Geusic, A.C. Puiu, J.B. Hopkins, T.G. Dietz, M.A. Duncan, P.R.R. Langridge-Smith, and R.E. Smalley, J. Chem. Phys. 86, 2556 (1982).
- [11] D.E. Powers, S.G.Hansen, M.E. Geusic, D.L. Michalopoulos, and R.E. Smalley, J.Chem. Phys. 78, 2866 (1983).
- [12] M.D. Morse, G.P. Hansen, P.R.R. Langridge-Smith, L.-S. Zheng, M.E. Geusic, D.L. Michalopoulos, R.E. Smalley, J. Chem. Phys. 80, 5400 (1984).
- [13] P.J. Brucat, L.-S. Zheng, C.L. Pettiette, S.Yang, and R.E. Smalley, J. Chem. Phys. 84, 3078 (1986).

- [14] J.L. Gole, J.H. English, and V.E. Bondybey, J. Chem. Phys. 86, 2560 (1982).
- [15] D.R. Preuss, S.A. Pace, and J.L. Gole, J. Chem. Phys. 71, 3553 (1979).
- [16] V.E. Bondybey, G.P. Schwartz, and J.H. English, J. Chem. Phys. 78, 11 (1983).
- [17] E.A. Rohlfing and J.J. Valentini, J. Chem. Phys. 84, 6560 (1986).
- [18] A.D. Sappes, J.E. Harrington, and J.C. Weisshaar, J. Chem. Phys. 88, 5243 (1988).
- [19] D.G. Leopold, J. Ho, and W.C. Lineberger, J. Chem. Phys. 86, 1715 (1987).
- [20] O. Cheshnovsky, P.J. Brucat, S. Yang, C.L. Pettiette, M.J. Craycraft, and R.E. Smalley, in Physics and Chemistry of Small Clusters, edited by P. Jena, B.K. Rao, and S.N. Khanna Plenum, New York, (1987), NATO ASI Series B: Physics, Vol. 158,p.1.
- [21] L. D. Marks, Rep. Prog. Phys. 57, 603 (1994).
- [22] G. Schmid, V. Maihack, F. Lantermann and S. Peschel, J. Chem. Soc., Dalton Trans. 589 (1996).
- [23] G. M. Francis, I. M. Goldby, L. Kuipers, B. von Issendorf and R. E. Palmer, J. Chem. Soc., Dalton Trans. 665 (1996).
- [24] R.P. Feynman, Talk at the annual meeting of the American Physical Society at the California Institute of Technology (Caltech), December 29th, (1959).
- [25] W. Eberhardt, Surf. Sci., 500, 242 (2002).
- [26] A.F. Voter, Los Alamos Unclassified Technical Report #LA-UR 93-3901 (1993).
- [27] K. Balasubramanian, J. Chem. Phys. 87, 6573 (1987).
- [28] J.E. Jones and A.E. Ingham, Proc. R. Soc. A 107, 636 (1925).
- [29] P.M. Morse, Phys. Rev. 34, 57 (1929).
- [30] B.M. Axilrod and E. Teller, J. Chem. Phys. 11, 299 (1943).
- [31] J.N. Murrell and R.E. Mottram, Mol. Phys. 69, 571 (1990).
- [32] M.W. Finnis and J.E. Sinclair, Philos. Mag. A 50, 45 (1984).
- [33] A. P. Sutton, and J. Chen, Philos. Mag. Lett. 61, 139 (1990).
- [34] F. Cleri and V. Rosato, Phys. Rev. B 48, 22 (1993).

- [35] M.S. Daw, and M.I. Baskes, Phys. Rev. B 29, 6443 (1984).
- [36] Z.B. Güvenç, and J. Jellinek, Z. Phys. D 26, 304 (1993).
- [37] Z.B. Güvenç, J. Jellinek, and A.F. Voter, Physics and Chemistry of Finite Systems: From Clusters to Crystals, Vol.1, p.411, Kluwer Academic Publishers, Dordrecht (1992).
- [38] M. Boyukata, Z.B. Güvenç, S. Özçelik, P. Durmuş, J. Jellinek, Int. J. Quantum Chem. 84, 208 (2001).
- [39] M.P. Allen and D.J. Tildesley, Computer Simulation of Liquids, Oxford Science Publications, (1987).
- [40] D.J. Wales and J.P.K. Doye, J. Phys. Chem. A, 101, 5111 (1997).
- [41] D.M. Deaven and K.M. Ho, Phys. Rev. Lett. 75, 288 (1995).
- [42] D.M. Deaven, N. Tit, J.R. Morris, and K.M. Ho, Chem. Phys. Lett. 256, 195 (1996).
- [43] F.R. Manby, R.L. Johnston, and C. Roberts, MATCH 38, 11 (1998).
- [44] C. Roberts, R.L. Johnston, and N.T. Wilson, Theor. Chem. Acc. 104, 123 (2000).
- [45] S. Taylor, G. W. Lemire, Y. M. Hamrick, Z. Fu, and M. D. Morse, J. Chem. Phys. 89, 5517 (1988).
- [46] K. Jansson, R. Scullman, J. Mol. Spectrosc. 61, 299 (1976).
- [47] S.K. Gupta, B.M. Nappi, and K.A. Gingerich, Inorg. Chem. 20, 966 (1981).
- [48] A. Sachdev, R.I. Masel, and J.B. Adams, J. Catal. 136, 320 (1992).
- [49] J.E. Sinclair, and R. Fletcher, J. Phys.C 7, 864 (1974).
- [50] J. Garcia-Rodeja, C. Rey, L.J. Galleo, and J.A. Alonso, Phys. Rev. B 49, 8495 (1994).
- [51] L. Yang, and A. E. DePristo, J. Chem. Phys. 100, 725 (1994).
- [52] M.S. Stave, D.E. Sanders, T.J. Raeker, and A. E. Depristo, J. Chem. Phys. 93, 4413 (1990).
- [53] J. P. K. Doye, and D. J. Wales, New J. Chem. 733 (1998).
- [54] Z. Li, and H. A. Scheraga, Proc. Natl. Acad. Sci. USA. 84, 6611 (1987).
- [55] C. MAssen, T.V. Mortimer-Jones and Roy L. Johnston, J. Chem. Soc., Dalton Trans. 23, 4375 (2002).

- [56] D.E. Ellis, J. Guo, H.P. Cheng, and J.J. Low, *Adv. Quantum Chem.* 22, 125 (1991).
- [57] D. Dai, and K. Balasubramanian, *J. Chem. Phys.* 103, 648 (1995).
- [58] S.H. Yang, D.A. Drabold, J.B. Adams, P. Ordejon, and K. Glassford, *J. Phys.: Condens. Matter* 9, L39 (1997).
- [59] J. Harris, *Phys. Rev. B* 31, 1770 (1987).
- [60] A. Fortunelli, *J. Molecular Structure (Theochem)*, 493, 223 (1999).
- [61] Amsterdam Density Functional (ADF), Revision 2.3.0, Theoretical Chemistry, Vrije Universiteit, Amsterdam (1997).
- [62] E. Apra, and A. Fortunelli, *J. Molecular Structure (Theochem)*, 501-502, 251 (2000).
- [63] D.E. Bernholt, E. Apra, H.A. Früchtl, M.F. Guest, R.J. Harrison, R.A. Kendall, R.A. Kutteh, X. Long, J.B. Fann, R.J. Littlefield, J. Nieplocha, *Int. J. Quantum Chem. Quantum Chem. Symp.* 29, 475 (1995).
- [64] C. Kittel, *Introduction to solid state physics* (seventh edition), John Wiley and Sons, USA, (1996).
- [65] Z.B. Güvenç, D. Güvenç, J. Jellinek, *Math. Comp. App.*, 4, 75 (1999).
- [66] M. Karabacak, S. Özçelik, and Z. B. Güvenç, *Surf. Sci.*, 507, 634 (2002).
- [67] M. Karabacak, S. Özçelik and Z.B. Güvenç, *Surf. Sci.*, 532-535, 306 (2003).
- [68] S. Özçelik and Z.B. Güvenç, *Surf. Sci.*, 532-535, 312 (2003).
- [69] R.H. Leary, *J. Glob. Opt.*, 18, 367 (2000).
- [70] J.P.K. Doye, M.A. Miller and D.J. Wales, *J. Chem. Phys.* 111, 8417 (1999).
- [71] R.H. Byrd, P. Lu, J. Nocedal and C. Zhu *SIAM J. Scientific Computing* 16, 1190 (1995).
- [72] <http://www-wales.ch.cam.ac.uk/software.html>.
- [73] J.A. Northby, J. Xie, D.L. Freeman, J.D. Doll, *Z. Phys. D* 12, 69 (1989).
- [74] J.W. Lee, G.D. Stein, *J. Phys. Chem.* 91, 2450 (1987).
- [75] K. Clemenger, *Phys. Rev. B* 32, 1359 (1985).
- [76] Y.J. Lee, E.K. Lee and S. Kim, *Pyhs. Rev. Lett.*, 86, 999 (2001).
- [77] A.L. Mackay, *Acta Crystallogr.*, 15, 916 (1962).

- [78] A. Sebetci and Z.B. Güvenç, Surf. Sci., 525, 66 (2003).
- [79] N.T. Wilson, and R.L. Johnston, Eur. Phys. J. D, 12, 161 (2000).
- [80] J. Uppenbrink and D.J. Wales, J. Chem. Pyhs., 96, 8520 (1992).
- [81] M. Andersson and A. Rosen, J. Chem. Pyhs., 117, 7501 (2002).
- [82] E.K. Parks, L. Zhu, J. Ho, and S.J. Riley, J. Chem. Pyhs., 100, 7206 (1994).
- [83] E.K. Parks, G.C. Nieman, K.P. Kerns, and S.J. Riley, J. Chem. Pyhs., 108, 3731 (1998).
- [84] E.K. Parks, and S.J. Riley, Z. Pyhs. D, 33, 59 (1995).
- [85] E.K. Parks, B.J. Winter, T.D. Klots, and S.J. Riley, J. Chem. Pyhs., 94, 1882 (1991).
- [86] N.T. Wilson, and R.L. Johnston, Phys. Chem. Chem. Phys., 4, 4168 (2002).
- [87] <http://brian.ch.cam.ac.uk/CCD.html>.
- [88] E.M. Pearson, T. Halicioglu and W.A. Tiller, Phys. Rev. A 32, 3030 (1985).
- [89] J. Jellinek and A. Goldberg, J. Chem. Phys. 113, 2570 (2000).
- [90] H.P. Chang and R.S.Berry, Phys. Rev. A, 45, 7969 (1992).
- [91] Y.J. Lee, J.Y. Maeng, E.K. Lee, B. Kim, S. Kim, K.K. Han, J. Comput. Chem., 21, 380, (2000).
- [92] Y.J. Lee, E.K. Lee, S. Kim, R.M. Nieminen, Phys. Rev. Lett. 86, 999, (2001).
- [93] Y. Chushak, and L.S. Bartell, Eur. Phys. J. D 16, 43 (2001).
- [94] F. Baletto, R. Ferrando, A. Fortunelli, F. Montalenti, and C. Mottet, J. Chem. Phys. 116, 3856 (2002).
- [95] L.D. Marks, Philop. Mag. A 49, 81 (1984).
- [96] F. Baletto, C. Mottet and R. Ferrando, Phys. Rev. Lett. 84, 5544 (2000).

VITA

He was born in Ermenek (Karaman) on January 27, 1972. He has received his bachelor's degree in Teaching Physics and master's degree in Physics from Boğaziçi University in February 1994 and April 1999, respectively. He has married in 1997. Just after completing the master's program he has been accepted as a Ph.D. student at the Physics Department of Middle East Technical University in the same year. He works as an instructor at the Computer Engineering Department of Çankaya University since September 2000.

PUBLICATIONS

The work contained in this thesis has been published or submitted to the publication in the following papers:

1. Energetics and structures of small clusters: Pt_N , $N = 2 - 21$, A. Sebetci and Z.B. Güvenç, Surf. Sci., 525, 66 (2003).
2. Global minima for free Pt_N clusters ($N = 22 - 56$): a molecular dynamics study, A. Sebetci and Z.B. Güvenç, J. Phys. B, submitted.
3. Molecular dynamics simulation of the melting behavior of 12-, 13-, 14-atom icosahedral platinum clusters, A. Sebetci and Z.B. Güvenç, Surf. Sci., submitted.
4. Melting behavior of icosahedral 54-, 55-, 56-atom platinum clusters, A. Sebetci, Z.B. Güvenç and H. Kökten, Appl. Surf. Sci., submitted.
5. Molecular dynamics simulation of Pt_{75} cluster: isomer spectrum and melting, Z.B. Güvenç and A. Sebetci, Eur. Phys. J. D, submitted.

Some of the results obtained during this study have been presented in the following conferences:

1. NATO-ASI, 09-20 September 2002, Varna, Bulgaria: *Computer Simulation of Surfaces and Interfaces*.
2. 09-10 April 2003, Mansfield College, Oxford, UK: *Modelling of Materials: Atomistic and Ab Initio Approaches*.
3. ECOSS 22, 07-12 September 2003, Prague, Czech Republic: *22nd European Conference on Surface Science*.
4. MSSC2003, 07-12 September 2003, Torino, Italy: *International School of Advanced Study of the University of Torino: Ab initio modeling in Solid State Chemistry*.
5. APHYS-2003, 14-18 October 2003, Badajoz, Spain: *First International Meeting on Applied Physics*.